

# Charged Particle Multiplicity in Three-Jet Events and Two-Gluon Systems

DELPHI Collaboration

## Abstract

The charged particle multiplicity in hadronic three-jet events from  $Z$  decays is investigated. The topology dependence of the event multiplicity is found to be well described by a modified leading logarithmic prediction. A parameter fit of the prediction to the data yields a measurement of the colour factor ratio  $C_A/C_F$  with the result

$$C_A/C_F = 2.261 \pm 0.014_{\text{stat.}} \pm 0.036_{\text{exp.}} \pm 0.066_{\text{theo.}}$$

in agreement with the SU(3) expectation of QCD. The quark-related contribution to the event multiplicity is subtracted from the three-jet event multiplicity resulting in a measurement of the multiplicity of two-gluon colour-singlet states over a wide energy range. The ratios  $r = N_{gg}(s)/N_{q\bar{q}}(s)$  of the gluon and quark multiplicities and  $r^{(1)} = N'_{gg}(s)/N'_{q\bar{q}}(s)$  of their derivatives are compared with perturbative calculations. While a good agreement between calculations and data is observed for  $r^{(1)}$ , larger deviations are found for  $r$  indicating that non-perturbative effects are more important for  $r$  than for  $r^{(1)}$ .

J.Abdallah<sup>25</sup>, P.Abreu<sup>22</sup>, W.Adam<sup>51</sup>, P.Adzic<sup>11</sup>, T.Albrecht<sup>17</sup>, T.Alderweireld<sup>2</sup>, R.Aleman-Fernandez<sup>8</sup>, T.Allmendinger<sup>17</sup>, P.P.Allport<sup>23</sup>, U.Amaldi<sup>29</sup>, N.Amapane<sup>45</sup>, S.Amato<sup>48</sup>, E.Anashkin<sup>36</sup>, A.Andrezza<sup>28</sup>, S.Andringa<sup>22</sup>, N.Anjos<sup>22</sup>, P.Antilogus<sup>25</sup>, W-D.Apel<sup>17</sup>, Y.Arnoud<sup>14</sup>, S.Ask<sup>26</sup>, B.Asman<sup>44</sup>, J.E.Augustin<sup>25</sup>, A.Augustinus<sup>8</sup>, P.Baillon<sup>8</sup>, A.Ballestrero<sup>46</sup>, P.Bambade<sup>20</sup>, R.Barbier<sup>27</sup>, D.Bardin<sup>16</sup>, G.J.Barker<sup>17</sup>, A.Baroncelli<sup>39</sup>, M.Battaglia<sup>8</sup>, M.Baillier<sup>25</sup>, K-H.Becks<sup>53</sup>, M.Begalli<sup>6</sup>, A.Behrmann<sup>53</sup>, E.Ben-Haim<sup>20</sup>, N.Benekos<sup>32</sup>, A.Benvenuti<sup>5</sup>, C.Berat<sup>14</sup>, M.Berggren<sup>25</sup>, L.Berntzon<sup>44</sup>, D.Bertrand<sup>2</sup>, M.Besancon<sup>40</sup>, N.Besson<sup>40</sup>, D.Bloch<sup>9</sup>, M.Blom<sup>31</sup>, M.Bluj<sup>52</sup>, M.Bonesini<sup>29</sup>, M.Boonekamp<sup>40</sup>, P.S.L.Booth<sup>23</sup>, G.Borisov<sup>21</sup>, O.Botner<sup>49</sup>, B.Bouquet<sup>20</sup>, T.J.V.Bowcock<sup>23</sup>, I.Boyko<sup>16</sup>, M.Bracko<sup>43</sup>, R.Brenner<sup>49</sup>, E.Brodet<sup>35</sup>, P.Bruckman<sup>18</sup>, J.M.Brunet<sup>7</sup>, P.Buschmann<sup>53</sup>, M.Calvi<sup>29</sup>, T.Camporesi<sup>8</sup>, V.Canale<sup>38</sup>, F.Carena<sup>8</sup>, N.Castro<sup>22</sup>, F.Cavallo<sup>5</sup>, M.Chapkin<sup>42</sup>, Ph.Charpentier<sup>8</sup>, P.Checchia<sup>36</sup>, R.Chierici<sup>8</sup>, P.Chliapnikov<sup>42</sup>, J.Chudoba<sup>8</sup>, S.U.Chung<sup>8</sup>, K.Cieslik<sup>18</sup>, P.Collins<sup>8</sup>, R.Contri<sup>13</sup>, G.Cosme<sup>20</sup>, F.Cossutti<sup>47</sup>, M.J.Costa<sup>50</sup>, D.Crennell<sup>37</sup>, J.Cuevas<sup>34</sup>, J.D'Hondt<sup>2</sup>, J.Dalmau<sup>44</sup>, T.da Silva<sup>48</sup>, W.Da Silva<sup>25</sup>, G.Della Ricca<sup>47</sup>, A.De Angelis<sup>47</sup>, W.De Boer<sup>17</sup>, C.De Clercq<sup>2</sup>, B.De Lotto<sup>47</sup>, N.De Maria<sup>45</sup>, A.De Min<sup>36</sup>, L.de Paula<sup>48</sup>, L.Di Ciaccio<sup>38</sup>, A.Di Simone<sup>39</sup>, K.Doroba<sup>52</sup>, J.Drees<sup>53,8</sup>, G.Eigen<sup>4</sup>, T.Ekelof<sup>49</sup>, M.Ellert<sup>49</sup>, M.Elsing<sup>8</sup>, M.C.Espirito Santo<sup>22</sup>, G.Fanourakis<sup>11</sup>, D.Fassouliotis<sup>11,3</sup>, M.Feindt<sup>17</sup>, J.Fernandez<sup>41</sup>, A.Ferrer<sup>50</sup>, F.Ferro<sup>13</sup>, U.Flagmeyer<sup>53</sup>, H.Foeth<sup>8</sup>, E.Fokitis<sup>32</sup>, F.Fulda-Quenzer<sup>20</sup>, J.Fuster<sup>50</sup>, M.Gandelman<sup>48</sup>, C.Garcia<sup>50</sup>, Ph.Gavillet<sup>8</sup>, E.Gazis<sup>32</sup>, R.Gokiel<sup>8,52</sup>, B.Golob<sup>43</sup>, G.Gomez-Ceballos<sup>41</sup>, P.Goncalves<sup>22</sup>, E.Graziani<sup>39</sup>, G.Grosdidier<sup>20</sup>, K.Grzelak<sup>52</sup>, J.Guy<sup>37</sup>, C.Haag<sup>17</sup>, A.Hallgren<sup>49</sup>, K.Hamacher<sup>53</sup>, K.Hamilton<sup>35</sup>, S.Haug<sup>33</sup>, F.Hauler<sup>17</sup>, V.Hedberg<sup>26</sup>, M.Hennecke<sup>17</sup>, H.Herr<sup>†8</sup>, J.Hoffman<sup>52</sup>, S-O.Holmgren<sup>44</sup>, P.J.Holt<sup>8</sup>, M.A.Houlden<sup>23</sup>, K.Hultqvist<sup>44</sup>, J.N.Jackson<sup>23</sup>, G.Jarlskog<sup>26</sup>, P.Jarry<sup>40</sup>, D.Jeans<sup>35</sup>, E.K.Johansson<sup>44</sup>, P.D.Johansson<sup>44</sup>, P.Jonsson<sup>27</sup>, C.Joram<sup>8</sup>, L.Jungermann<sup>17</sup>, F.Kapusta<sup>25</sup>, S.Katsanevas<sup>27</sup>, E.Katsoufis<sup>32</sup>, G.Kernel<sup>43</sup>, B.P.Kersevan<sup>8,43</sup>, U.Kerzel<sup>17</sup>, B.T.King<sup>23</sup>, N.J.Kjaer<sup>8</sup>, P.Kluit<sup>31</sup>, P.Kokkinias<sup>11</sup>, C.Kourkoumelis<sup>3</sup>, O.Kouznetsov<sup>16</sup>, Z.Krumstein<sup>16</sup>, M.Kucharczyk<sup>18</sup>, J.Lamsa<sup>1</sup>, G.Leder<sup>51</sup>, F.Ledroit<sup>14</sup>, L.Leinonen<sup>44</sup>, R.Leitner<sup>30</sup>, J.Lemonne<sup>2</sup>, V.Lepeltier<sup>20</sup>, T.Lesiak<sup>18</sup>, W.Liebig<sup>53</sup>, D.Liko<sup>51</sup>, A.Lipniacka<sup>44</sup>, J.H.Lopes<sup>48</sup>, J.M.Lopez<sup>34</sup>, D.Loukas<sup>11</sup>, P.Lutz<sup>40</sup>, L.Lyons<sup>35</sup>, J.MacNaughton<sup>51</sup>, A.Malek<sup>53</sup>, S.Maltezos<sup>32</sup>, F.Mandl<sup>51</sup>, J.Marco<sup>41</sup>, R.Marco<sup>41</sup>, B.Marechal<sup>48</sup>, M.Margoni<sup>36</sup>, J-C.Marin<sup>8</sup>, C.Mariotti<sup>8</sup>, A.Markou<sup>11</sup>, C.Martinez-Rivero<sup>41</sup>, J.Masik<sup>12</sup>, N.Mastroyiannopoulos<sup>11</sup>, F.Matorras<sup>41</sup>, C.Matteuzzi<sup>29</sup>, F.Mazzucato<sup>36</sup>, M.Mazzucato<sup>36</sup>, R.Mc Nulty<sup>23</sup>, C.Meroni<sup>28</sup>, E.Migliore<sup>45</sup>, W.Mitaroff<sup>51</sup>, U.Mjoernmark<sup>26</sup>, T.Moa<sup>44</sup>, M.Moch<sup>17</sup>, K.Moenig<sup>8,10</sup>, R.Monge<sup>13</sup>, J.Montenegro<sup>31</sup>, D.Moraes<sup>48</sup>, S.Moreno<sup>22</sup>, P.Morettini<sup>13</sup>, U.Mueller<sup>53</sup>, K.Muenich<sup>53</sup>, M.Mulders<sup>31</sup>, L.Mundim<sup>6</sup>, W.Murray<sup>37</sup>, B.Muryn<sup>19</sup>, G.Myatt<sup>35</sup>, T.Myklebust<sup>33</sup>, M.Nassiakou<sup>11</sup>, F.Navarria<sup>5</sup>, K.Nawrocki<sup>52</sup>, R.Nicolaidou<sup>40</sup>, M.Nikolenko<sup>16,9</sup>, A.Oblakowska-Mucha<sup>19</sup>, V.Obratzov<sup>42</sup>, A.Olshevski<sup>16</sup>, A.Onofre<sup>22</sup>, R.Orava<sup>15</sup>, K.Osterberg<sup>15</sup>, A.Ouraou<sup>40</sup>, A.Oyanguren<sup>50</sup>, M.Paganoni<sup>29</sup>, S.Paiano<sup>5</sup>, J.P.Palacios<sup>23</sup>, H.Palka<sup>18</sup>, Th.D.Papadopoulou<sup>32</sup>, L.Pape<sup>8</sup>, C.Parkes<sup>24</sup>, F.Parodi<sup>13</sup>, U.Parzefall<sup>8</sup>, A.Passeri<sup>39</sup>, O.Passon<sup>53</sup>, L.Peralta<sup>22</sup>, V.Perepelitsa<sup>50</sup>, A.Perrotta<sup>5</sup>, A.Petrolini<sup>13</sup>, J.Piedra<sup>41</sup>, L.Pieri<sup>39</sup>, F.Pierre<sup>40</sup>, M.Pimenta<sup>22</sup>, E.Piotto<sup>8</sup>, T.Podobnik<sup>43</sup>, V.Poireau<sup>8</sup>, M.E.Pol<sup>6</sup>, G.Polok<sup>18</sup>, V.Pozdniakov<sup>16</sup>, N.Pukhaeva<sup>2,16</sup>, A.Pullia<sup>29</sup>, J.Rames<sup>12</sup>, A.Read<sup>33</sup>, P.Rebecchi<sup>8</sup>, J.Rehn<sup>17</sup>, D.Reid<sup>31</sup>, R.Reinhardt<sup>53</sup>, P.Renton<sup>35</sup>, F.Richard<sup>20</sup>, J.Ridky<sup>12</sup>, M.Rivero<sup>41</sup>, D.Rodriguez<sup>41</sup>, A.Romero<sup>45</sup>, P.Ronchese<sup>36</sup>, P.Roudeau<sup>20</sup>, T.Rovelli<sup>5</sup>, V.Ruhlmann-Kleider<sup>40</sup>, D.Ryabtchikov<sup>42</sup>, A.Sadovsky<sup>16</sup>, L.Salmi<sup>15</sup>, J.Salt<sup>50</sup>, C.Sander<sup>17</sup>, A.Savoy-Navarro<sup>25</sup>, U.Schwickerath<sup>8</sup>, A.Segar<sup>†35</sup>, R.Sekulin<sup>37</sup>, M.Siebel<sup>53</sup>, A.Sisakian<sup>16</sup>, G.Smadja<sup>27</sup>, O.Smirnova<sup>26</sup>, A.Sokolov<sup>42</sup>, A.Sopczak<sup>21</sup>, R.Sosnowski<sup>52</sup>, T.Spaso<sup>8</sup>, M.Stanitzki<sup>17</sup>, A.Stocchi<sup>20</sup>, J.Strauss<sup>51</sup>, B.Stugu<sup>4</sup>, M.Szczekowski<sup>52</sup>, M.Szeptycka<sup>52</sup>, T.Szumlak<sup>19</sup>, T.Tabarelli<sup>29</sup>, A.C.Taffard<sup>23</sup>, F.Tegenfeldt<sup>49</sup>, J.Timmermans<sup>31</sup>, L.Tkatchev<sup>16</sup>, M.Tobin<sup>23</sup>, S.Todorovova<sup>12</sup>, B.Tome<sup>22</sup>, A.Tonazzo<sup>29</sup>, P.Tortosa<sup>50</sup>, P.Travnicek<sup>12</sup>, D.Treille<sup>8</sup>, G.Tristram<sup>7</sup>, M.Trochimczuk<sup>52</sup>, C.Troncon<sup>28</sup>, M-L.Turluer<sup>40</sup>, I.A.Tyapkin<sup>16</sup>, P.Tyapkin<sup>16</sup>, S.Tzamarias<sup>11</sup>, V.Uvarov<sup>42</sup>, G.Valenti<sup>5</sup>, P.Van Dam<sup>31</sup>, J.Van Eldik<sup>8</sup>, N.van Remortel<sup>15</sup>, I.Van Vulpen<sup>8</sup>, G.Vegni<sup>28</sup>, F.Veloso<sup>22</sup>, W.Venus<sup>37</sup>, P.Verdier<sup>27</sup>, V.Verzi<sup>38</sup>, D.Vilanova<sup>40</sup>, L.Vitale<sup>47</sup>, V.Vrba<sup>12</sup>, H.Wahlen<sup>53</sup>, A.J.Washbrook<sup>23</sup>, C.Weiser<sup>17</sup>, D.Wicke<sup>8</sup>, J.Wickens<sup>2</sup>,

G.Wilkinson<sup>35</sup>, M.Winter<sup>9</sup>, M.Witek<sup>18</sup>, O.Yushchenko<sup>42</sup>, A.Zalewska<sup>18</sup>, P.Zalewski<sup>52</sup>, D.Zavrtanik<sup>43</sup>, V.Zhuravlov<sup>16</sup>, N.I.Zimin<sup>16</sup>, A.Zintchenko<sup>16</sup>, M.Zupan<sup>11</sup>

- 
- <sup>1</sup>Department of Physics and Astronomy, Iowa State University, Ames IA 50011-3160, USA  
<sup>2</sup>Physics Department, Universiteit Antwerpen, Universiteitsplein 1, B-2610 Antwerpen, Belgium and IIHE, ULB-VUB, Pleinlaan 2, B-1050 Brussels, Belgium  
and Faculté des Sciences, Univ. de l'Etat Mons, Av. Maistriau 19, B-7000 Mons, Belgium  
<sup>3</sup>Physics Laboratory, University of Athens, Solonos Str. 104, GR-10680 Athens, Greece  
<sup>4</sup>Department of Physics, University of Bergen, Allégaten 55, NO-5007 Bergen, Norway  
<sup>5</sup>Dipartimento di Fisica, Università di Bologna and INFN, Via Irnerio 46, IT-40126 Bologna, Italy  
<sup>6</sup>Centro Brasileiro de Pesquisas Físicas, rua Xavier Sigaud 150, BR-22290 Rio de Janeiro, Brazil and Depto. de Física, Pont. Univ. Católica, C.P. 38071 BR-22453 Rio de Janeiro, Brazil  
and Inst. de Física, Univ. Estadual do Rio de Janeiro, rua São Francisco Xavier 524, Rio de Janeiro, Brazil  
<sup>7</sup>Collège de France, Lab. de Physique Corpusculaire, IN2P3-CNRS, FR-75231 Paris Cedex 05, France  
<sup>8</sup>CERN, CH-1211 Geneva 23, Switzerland  
<sup>9</sup>Institut de Recherches Subatomiques, IN2P3 - CNRS/ULP - BP20, FR-67037 Strasbourg Cedex, France  
<sup>10</sup>Now at DESY-Zeuthen, Platanenallee 6, D-15735 Zeuthen, Germany  
<sup>11</sup>Institute of Nuclear Physics, N.C.S.R. Demokritos, P.O. Box 60228, GR-15310 Athens, Greece  
<sup>12</sup>FZU, Inst. of Phys. of the C.A.S. High Energy Physics Division, Na Slovance 2, CZ-180 40, Praha 8, Czech Republic  
<sup>13</sup>Dipartimento di Fisica, Università di Genova and INFN, Via Dodecaneso 33, IT-16146 Genova, Italy  
<sup>14</sup>Institut des Sciences Nucléaires, IN2P3-CNRS, Université de Grenoble 1, FR-38026 Grenoble Cedex, France  
<sup>15</sup>Helsinki Institute of Physics and Department of Physical Sciences, P.O. Box 64, FIN-00014 University of Helsinki, Finland  
<sup>16</sup>Joint Institute for Nuclear Research, Dubna, Head Post Office, P.O. Box 79, RU-101 000 Moscow, Russian Federation  
<sup>17</sup>Institut für Experimentelle Kernphysik, Universität Karlsruhe, Postfach 6980, DE-76128 Karlsruhe, Germany  
<sup>18</sup>Institute of Nuclear Physics PAN,Ul. Radzikowskiego 152, PL-31142 Krakow, Poland  
<sup>19</sup>Faculty of Physics and Nuclear Techniques, University of Mining and Metallurgy, PL-30055 Krakow, Poland  
<sup>20</sup>Université de Paris-Sud, Lab. de l'Accélérateur Linéaire, IN2P3-CNRS, Bât. 200, FR-91405 Orsay Cedex, France  
<sup>21</sup>School of Physics and Chemistry, University of Lancaster, Lancaster LA1 4YB, UK  
<sup>22</sup>LIP, IST, FCUL - Av. Elias Garcia, 14-1<sup>o</sup>, PT-1000 Lisboa Codex, Portugal  
<sup>23</sup>Department of Physics, University of Liverpool, P.O. Box 147, Liverpool L69 3BX, UK  
<sup>24</sup>Dept. of Physics and Astronomy, Kelvin Building, University of Glasgow, Glasgow G12 8QQ  
<sup>25</sup>LPNHE, IN2P3-CNRS, Univ. Paris VI et VII, Tour 33 (RdC), 4 place Jussieu, FR-75252 Paris Cedex 05, France  
<sup>26</sup>Department of Physics, University of Lund, Sölvegatan 14, SE-223 63 Lund, Sweden  
<sup>27</sup>Université Claude Bernard de Lyon, IPNL, IN2P3-CNRS, FR-69622 Villeurbanne Cedex, France  
<sup>28</sup>Dipartimento di Fisica, Università di Milano and INFN-MILANO, Via Celoria 16, IT-20133 Milan, Italy  
<sup>29</sup>Dipartimento di Fisica, Univ. di Milano-Bicocca and INFN-MILANO, Piazza della Scienza 2, IT-20126 Milan, Italy  
<sup>30</sup>IPNP of MFF, Charles Univ., Areal MFF, V Holesovickach 2, CZ-180 00, Praha 8, Czech Republic  
<sup>31</sup>NIKHEF, Postbus 41882, NL-1009 DB Amsterdam, The Netherlands  
<sup>32</sup>National Technical University, Physics Department, Zografou Campus, GR-15773 Athens, Greece  
<sup>33</sup>Physics Department, University of Oslo, Blindern, NO-0316 Oslo, Norway  
<sup>34</sup>Dpto. Física, Univ. Oviedo, Avda. Calvo Sotelo s/n, ES-33007 Oviedo, Spain  
<sup>35</sup>Department of Physics, University of Oxford, Keble Road, Oxford OX1 3RH, UK  
<sup>36</sup>Dipartimento di Fisica, Università di Padova and INFN, Via Marzolo 8, IT-35131 Padua, Italy  
<sup>37</sup>Rutherford Appleton Laboratory, Chilton, Didcot OX11 0QX, UK  
<sup>38</sup>Dipartimento di Fisica, Università di Roma II and INFN, Tor Vergata, IT-00173 Rome, Italy  
<sup>39</sup>Dipartimento di Fisica, Università di Roma III and INFN, Via della Vasca Navale 84, IT-00146 Rome, Italy  
<sup>40</sup>DAPNIA/Service de Physique des Particules, CEA-Saclay, FR-91191 Gif-sur-Yvette Cedex, France  
<sup>41</sup>Instituto de Física de Cantabria (CSIC-UC), Avda. los Castros s/n, ES-39006 Santander, Spain  
<sup>42</sup>Inst. for High Energy Physics, Serpukov P.O. Box 35, Protvino, (Moscow Region), Russian Federation  
<sup>43</sup>J. Stefan Institute, Jamova 39, SI-1000 Ljubljana, Slovenia and Laboratory for Astroparticle Physics, Nova Gorica Polytechnic, Kostanjevska 16a, SI-5000 Nova Gorica, Slovenia, and Department of Physics, University of Ljubljana, SI-1000 Ljubljana, Slovenia  
<sup>44</sup>Fysikum, Stockholm University, Box 6730, SE-113 85 Stockholm, Sweden  
<sup>45</sup>Dipartimento di Fisica Sperimentale, Università di Torino and INFN, Via P. Giuria 1, IT-10125 Turin, Italy  
<sup>46</sup>INFN, Sezione di Torino and Dipartimento di Fisica Teorica, Università di Torino, Via Giuria 1, IT-10125 Turin, Italy  
<sup>47</sup>Dipartimento di Fisica, Università di Trieste and INFN, Via A. Valerio 2, IT-34127 Trieste, Italy and Istituto di Fisica, Università di Udine, IT-33100 Udine, Italy  
<sup>48</sup>Univ. Federal do Rio de Janeiro, C.P. 68528 Cidade Univ., Ilha do Fundão BR-21945-970 Rio de Janeiro, Brazil  
<sup>49</sup>Department of Radiation Sciences, University of Uppsala, P.O. Box 535, SE-751 21 Uppsala, Sweden  
<sup>50</sup>IFIC, Valencia-CSIC, and D.F.A.M.N., U. de Valencia, Avda. Dr. Moliner 50, ES-46100 Burjassot (Valencia), Spain  
<sup>51</sup>Institut für Hochenergiephysik, Österr. Akad. d. Wissensch., Nikolsdorfergasse 18, AT-1050 Vienna, Austria  
<sup>52</sup>Inst. Nuclear Studies and University of Warsaw, Ul. Hoza 69, PL-00681 Warsaw, Poland  
<sup>53</sup>Fachbereich Physik, University of Wuppertal, Postfach 100 127, DE-42097 Wuppertal, Germany

† deceased

# 1 Introduction

Abundant particle multiplicity is one of the most obvious properties of hadronic final states in  $e^+e^-$  annihilation. The reason for the large multiplicity of particles produced in hadronic events is directly rooted to one of the fundamental properties of the strong interaction: the confinement of quarks and gluons into hadrons. Unlike leptons, quarks produced in a high energy reaction are not able just to separate without further interactions in which the colour charges are balanced and free colour singlets are formed. Ironically, it is the very same property of QCD which makes it impossible to predict the average number of hadrons produced in such an event. However, the hypothesis of Local Parton-Hadron Duality (LPHD) allows the assumption to be made that the hadronic multiplicity of an event is related only via a normalisation factor to the partonic multiplicity at a given virtuality cut-off  $Q_0$ , which then is a perturbatively calculable quantity.

The multiplicity of  $q\bar{q}$  colour-singlet systems is well understood in this way. Theoretical predictions of the energy dependence of the multiplicity produced in such systems [1–3] have been confirmed by experimental data to high accuracy [4–6]. It is possible to predict the multiplicity of two-gluon colour-singlet systems perturbatively in a similar fashion, but experimental verification of this quantity is scarce. Two-gluon systems are experimentally difficult to produce and are observed so far only in decays of resonances with relatively low mass. The ratio of the multiplicity of quark and gluon systems,  $r$ , has been subject to theoretical studies presented in Sect. 3. It is expected that  $r$  at high energies resembles asymptotically the colour factor ratio  $C_A/C_F$ .  $C_F$  and  $C_A$ , which are the Casimir eigenvalues of the triplet and octet representation of  $SU(3)$ , can be interpreted as effective colour charges of the triplet quarks and the octet gluons. However,  $r$  is known to have large corrections in higher orders of the perturbative expansion and moreover, is supposed to be affected by non-perturbative effects. Therefore, the ratio of the derivatives of the quark and gluon multiplicities with respect to energy,  $r^{(1)}$ , has been suggested in [7] as a better suited observable.

The next slightly more complex class of events which can be studied in  $e^+e^-$  annihilation are events with three jets, which occur if in a  $q\bar{q}$ -event a gluon is radiated with a sufficiently large transverse momentum. Three-jet events are unique in the sense that they provide quark jets as well as gluon jets and therefore provide the opportunity to study the properties of gluon fragmentation once the  $q\bar{q}$ -contributions are understood. There have been numerous experimental studies where the properties of identified quark and gluon jets are compared (e.g. [8–12]). A crucial question arising in this context is how the environment of a three-jet event affects the properties of a quark or gluon jet compared to the unrestricted jets of a  $q\bar{q}$ - or two-gluon event in terms of phase space restriction or coherent radiation. Studies have been made to verify experimentally several proper energy scale like variables which account for these differences by applying the appropriate evaluation scales for the jets in three-jet events (e.g. in [9,11]). Coherence effects in the particle production in three-jet events have been subject to a recent study [13]. In parallel with the publication of an analysis of the charged multiplicity of symmetric three-jet events applying a rather phenomenological approach [14], a theoretical prediction of the multiplicity of three-jet events has been published [15,16], which is derived in the colour-dipole picture of the Modified Leading Logarithmic Approximation (MLLA) and takes into account the effects of colour coherence and phase-space restriction in a stringent way. This prediction has been applied to study the topology-dependence of the event multiplicity of symmetric three-jet events in [17] and later in [18].

In this paper this prediction is not only applied to the charged multiplicity of three-jet events of symmetric topologies, but events with more general topologies are also considered. In the following section the experiment, data selection and the classification of three-jet event topologies is laid out. Sect. 3 deals with the relevant theoretical predictions, before in Sect. 4 the measured multiplicities are discussed. The following section deals with the preparation of the predictions which are then compared to the data in Sect. 6. A parameter fit to determine the colour-factor ratio  $C_A/C_F$  is performed and the systematic uncertainties of this measurement are discussed. In Sect. 7 the prediction is used to extract the multiplicity of two-gluon colour singlet systems from the three-jet event multiplicity by subtracting the quark contribution. With the measurements of the charged two-gluon multiplicity  $N_{gg}$  the ratios  $r$  and  $r^{(1)}$  are evaluated and the possibility of measuring the ratio of the second derivatives,  $r^{(2)}$ , is studied. The summary and conclusions are presented in Sect. 8.

## 2 Data and data analysis

variable	cut
$p$	$\geq 0.4 \text{ GeV}$
$\vartheta_{\text{polar}}$	$20^\circ - 160^\circ$
$\epsilon_{xy}$	$\leq 5 \text{ cm}$
$\epsilon_z$	$\leq 10 \text{ cm}$
$L_{\text{track}}$	$\geq 30 \text{ cm}$
$\Delta p/p$	$\leq 100\%$
$E_{\text{HPC}}$	$0.5 \text{ GeV} - 50 \text{ GeV}$
$E_{\text{EMF}}$	$0.5 \text{ GeV} - 50 \text{ GeV}$
$E_{\text{HAC}}$	$1 \text{ GeV} - 50 \text{ GeV}$

Table 1: Selection cuts applied to charged-particle tracks and to calorimeter clusters.

variable	cut
general events	
$E_{\text{charged}}^{\text{hemisph.}}$	$\geq 0.03 \cdot \sqrt{s}$
$E_{\text{charged}}^{\text{total}}$	$\geq 0.12 \cdot \sqrt{s}$
$N_{\text{charged}}$	$\geq 5$
$\vartheta_{\text{sphericity}}$	$30^\circ - 150^\circ$
$p_{\text{max}}$	$45 \text{ GeV}$
three-jet events	
$\sum_{i=1}^3 \theta_i$	$> 355^\circ$
$E_{\text{visible}}/\text{jet}$	$\geq 5 \text{ GeV}$
$N_{\text{charged}}/\text{jet}$	$\geq 2$
$\vartheta_{\text{jet}}$	$30^\circ - 150^\circ$

Table 2: Selection cuts applied to general events and to three-jet events.

In this paper the hadronic events from  $Z$  decays recorded by the DELPHI experiment in the years 1992-1995 are analysed. The DELPHI detector was a hermetic collider detector with a solenoidal magnetic field, extensive tracking facilities including a micro-vertex detector, electromagnetic and hadronic calorimetry as well as extended particle identification capabilities. The detector and its performance are described in detail elsewhere [19,20].

In order to select well-measured particles originating from the interaction point, the cuts shown in Tab. 1 were applied to the measured tracks and electromagnetic or hadronic calorimeter clusters. Here  $p$  and  $E$  denote the particle's momentum and energy,  $\vartheta_{\text{polar}}$  denotes the polar angle with respect to the beam,  $\epsilon_k$  is the distance of closest approach to the interaction point in the plane perpendicular to  $(xy)$  or along  $(z)$  the beam, respectively,  $L_{\text{track}}$  is the measured track length.  $E_{\text{HPC}}$  ( $E_{\text{EMF}}$ ) denotes the energy of a cluster as measured with the barrel (forward) electromagnetic calorimeter, and  $E_{\text{HAC}}$  the cluster energy measured by the hadronic calorimeter.

The general event cuts shown in Tab. 2 select hadronic decays of the  $Z$  and suppress background from leptonic  $Z$  decays,  $\gamma\gamma$  interactions or beam-gas interactions. Further

reduction of background to a negligible level is achieved by the jet-selection cuts given also in Tab. 2. The cut variables are the visible charged energy,  $E_{\text{charged}}^{\text{total}}$  and  $E_{\text{charged}}^{\text{hemisph.}}$ , observed in the event or in each event hemisphere, respectively. Event hemispheres are defined by the plane perpendicular to the sphericity axis. The polar angle of this axis with respect to the beam is  $\vartheta_{\text{sphericity}}$  and  $N_{\text{charged}}$  is the observed charged multiplicity. Events are discarded, if they contain charged particles with momenta apparently above the kinematic limit.

In addition to the event selection above, a procedure to tag events with initial  $b$ -quarks is applied. Details of the tagging procedure, which is based on the combined information of several observables, can be found in [21]. A cut on the tagging variable  $\lambda$  by demanding  $\lambda < 1.5$  is used to reject  $b$ -events leading to a light quark event purity of  $\sim 92\%$ . Both, the complete set of accepted hadronic ( $udscb$ -) events as well as the set of anti-tagged light ( $udsc$ -) quark events are analysed for cross-check reasons.

In the accepted events three jets are then reconstructed using the angular ordered Durham algorithm [22] taking into account reconstructed momenta of charged particles and of neutral particles seen in the electromagnetic calorimeter. No cut-off variable for the cluster algorithm is used, every event is clustered into three jets. For cross-check reasons, the Durham [23], Cambridge [22] and Luclus [24] jet clustering algorithms have been used alternatively<sup>1</sup>. As three-jet events have to be planar due to momentum conservation, the three reconstructed jets are projected into the event-plane, which is defined by the first two eigenvectors of the sphericity tensor [25].

The three-jet event quality requirements, also shown in Tab. 2, assure well-measured jets. Here  $\theta_i$  denotes the angle between the two jets opposite to jet  $i$ ,  $\vartheta_{\text{jet}}$  the polar angle of a jet and  $E_{\text{visible}}/\text{jet}$  the total visible energy per jet, taking into account all tracks and information from the electromagnetic calorimeter assigned to this jet. Assuming massless jet kinematics the topology of an event can be characterised by the three angles  $\theta_{1,2,3}$  between the jets. The inter-jet angles are ordered according to their size with  $\theta_1$  being the smallest and  $\theta_3$  the largest angle. This reflects the wide-spread convention due to which jets are numbered according to their energy with jet 1 being the most energetic, while the inter-jet angles are numbered according to their opposing jet. With massless jets this implies the numbering of the angles given above.

The inter-jet angles of the projected jets add up to  $360^\circ$ . Therefore giving two of the three angles is sufficient to fully determine the topology of an event. Here,  $\theta_2$  and  $\theta_3$  are used to define the binning. The angular intervals used to define bins of different topology classes are listed in Tab. 3. The allowed values for  $\theta_2$  depend on the value of  $\theta_3$ , as  $\theta_2 < \theta_3$  and  $\theta_2 > 180^\circ - \theta_3/2$ , the latter being a consequence of  $\theta_2 > \theta_1$ .

Besides these general classes of topologies, classes of *symmetric topologies* are selected, where symmetric events are defined by the requirement of the two larger inter-jet angles of an event,  $\theta_2$  and  $\theta_3$  to be equal within small tolerances, i.e.  $\theta_3 \leq \theta_2 + \Delta\theta$ . An angular tolerance less than  $5^\circ$  is not meaningful, as Monte Carlo studies showed that the differences between the inter-jet angles in the partonic and in the hadronic state scatter with a standard deviation of  $\sim 5^\circ$ . Therefore  $\Delta\theta = 5^\circ$  is chosen here. Since  $\theta_3$  has to be larger than  $120^\circ$ , the binning is completely determined by the choice of  $\Delta\theta$ . Symmetric events have been used in several previous studies (e.g. [8–11,14,17,18]), exploiting the special property of these events. With jet 2 and jet 3 being a quark and a gluon jet with exactly the same topological environment, a similar energy scale is present. Here symmetric topologies, which are also contained as a subset in the general event topologies,

<sup>1</sup>It is in the nature of the Cambridge algorithm, that depending on the structure of an event not every number of jets can be resolved. The small number of events where three jets could not be resolved are discarded when using the Cambridge algorithm.

$\theta_2$		$\theta_3$
98° – 100°	119° – 123°	120° – 130°
100° – 102°	123° – 128°	130° – 140°
102° – 104°	128° – 133°	140° – 145°
104° – 106°	133° – 138°	145° – 150°
106° – 108°	138° – 143°	150° – 155°
108° – 111°	143° – 148°	155° – 160°
111° – 115°	148° – 155°	160° – 165°
115° – 119°		

Table 3: The bins in  $\theta_2$  and  $\theta_3$ 

are studied also separately. Due to the additional constraint on symmetric topologies, giving only one inter-jet angle is sufficient to fully describe the topology of a symmetric event. For consistency with previous studies  $\theta_1$  is used for this purpose. The reduction to only one independent variable considerably simplifies most correction procedures. Note that the symmetric events are not fully contained in the general event topologies listed in Tab. 3, as the minimum value for  $\theta_1$  allowed by the binning in Tab. 3 is 40°. In symmetric events jet 3 is produced with maximum energy, therefore smaller opening angles  $\theta_1$  can be accepted. However, Monte Carlo studies showed that the resolved hadronic jet structure does not reflect the partonic structure of an event, if  $\theta_1$  is smaller than  $\sim 20^\circ$ , which therefore gives a lower boundary for  $\theta_1$ .

For each  $(\theta_2, \theta_3)$ -bin of the general topologies, and each  $\theta_1$ -bin of the symmetric event sample, the multiplicity distribution is measured. To correct these distributions for detector acceptance, a matrix correction is used. For each angular bin a matrix  $M_{mn}$  is calculated by tracing in a Monte Carlo simulation how many particles  $m$  in an accepted event with  $n$  detected particles have been generated. In order to obtain the generated number of charged particles, particles with lifetimes shorter than  $10^{-9}$ s, like  $K_S^0$  and  $\Lambda$ , have been forced to decay.  $M_{mn}$  is then applied to the measured distributions. Since generated events which fail to fulfil the selection criteria are not considered when calculating  $M_{mn}$  and these events are biased towards low multiplicities, the correction is slightly overestimated. In order to correct for this overestimation, the multiplicity distributions are multiplied by the ratio of the multiplicity distributions of all generated events with the multiplicity distributions of all generated and not rejected events for the respective angular bin. While the application of  $M_{mn}$  increases the mean of the distributions by  $\sim 30\%$ , the multiplicative second correction results in a reduction by only  $\sim 4\%$ .

When correcting the multiplicity distributions of *udsc*-events, the matrix corrected multiplicity distributions still contain some contributions due to mistagged *b*-events, which are not considered in the second multiplicative correction. Therefore the remaining contribution due to *b*-events is taken from the Monte Carlo simulation and subtracted from the matrix corrected distribution. This correction is small, the mean of the multiplicity distributions is changed by only  $\sim 0.6\%$ .

The central values for the results of the mean multiplicities as a function of the event topology are taken to be the arithmetic mean of the respective multiplicity distributions. However, in order to estimate the systematic effects of the correction procedure, two variations of the correction procedure are also applied:

- The mean multiplicity is determined from the expectation value of a negative binomial distribution fitted to every multiplicity distribution.

- Instead of correcting the distributions, the means of the uncorrected distributions are taken and corrected with a multiplicative factor taken from Monte Carlo simulation.

The corrected mean multiplicities obtained by using all three correction procedures agree well, the small variation is considered in the systematic errors of the analysis.

This procedure provides fully corrected mean multiplicities of hadronic three-jet events with initial  $udscb$ -quark – and  $udsc$ -quarks for cross-check reasons – as a function of the event topology for general and symmetric topologies. Additionally, the multiplicity distribution and mean multiplicity of all accepted events regardless of angular restrictions is treated in the same way to compare this measurement with previous measurements of this quantity. The events entering this overall multiplicity distribution are not required to fulfil the cuts on the jet structure given in the lower part of Tab. 2.

### 3 Theoretical Predictions

The ratio of gluon and quark multiplicities  $r$  has been subject to theoretical studies for some time. The naive expectation that this ratio reflects the ratio of the effective colour charges of quarks and gluons given by the colour factor ratio  $C_A/C_F$  is subject to large corrections. The multiplicity ratio

$$r = \frac{N_{gg}}{N_{q\bar{q}}} = r_0[1 - r_1\gamma_0 - r_2\gamma_0^2 - r_3\gamma_0^3] \quad (1)$$

is given as an expansion in the anomalous dimension  $\gamma_0$ , which can be expressed in terms of the strong coupling  $\alpha_s$  as

$$\gamma_0 = \sqrt{\frac{2C_A\alpha_s}{\pi}} \quad . \quad (2)$$

Here  $r_0$  denotes the colour factor ratio  $C_A/C_F$ , the coefficients  $r_i$  of the correction terms have been calculated in Leading Order (LO) ( $r_1$ ) [26], Next-to-Leading Order (NLO) ( $r_1, r_2$ ) [2] and, using a different approach in which energy conservation is considered, in Next-to-Next-to-Next-to-Leading Order (3NLO) ( $r_1, r_2$  and  $r_3$ ) [27]. As non-perturbative effects of the hadronisation process or energy conservation lead to large corrections for the ratio  $r$ , the suggestion has been made rather to study the ratio of the derivatives of the multiplicities with respect to the energy scale  $r^{(1)}$  [7] which should be less affected by non-perturbative effects. The ratio has been calculated in 3NLO [3] as

$$r^{(1)} = \frac{d \langle N_{gg} \rangle / ds}{d \langle N_{q\bar{q}} \rangle / ds} = \frac{r}{\rho_1} \quad (3)$$

with

$$\rho_1 = 1 - \frac{\beta_0}{8C_A} r_1 \gamma_0^2 \left[ 1 + \left( a_1 + r_1 + \frac{2r_2}{r_1} \right) \gamma_0 + \left( \frac{2r_2 a_1}{r_1} + a_1 r_1 + 3r_2 + \frac{3r_3}{r_1} + a_2 + a_1^2 + r_1^2 + \frac{\beta_1}{4C_A \beta_0} \right) \gamma_0^2 \right] \quad (4)$$

and  $r$  from Eqn. 1. The coefficients  $r_i$  and  $a_i$  have been calculated in [3] and are given in Tab. 4 and Tab. 5,  $\beta_0$  and  $\beta_1$  are the first two coefficients of the QCD  $\beta$ -function.

In another study [15] the ratio  $r^{(1)}$  has been derived in MLLA within the framework of the colour dipole model. It is implicitly expressed in the energy evolution of the gluon



multiplicity in relation to that of the quark multiplicity:

$$\left. \frac{dN_{gg}(L')}{dL'} \right|_{L'=L+c_g-c_q} = \frac{C_A}{C_F} \left( 1 - \frac{\alpha_0 c_r}{L} \right) \frac{d}{dL} N_{q\bar{q}}(L) \quad (5)$$

with

$$L = \ln \left( \frac{s}{\Lambda^2} \right) \quad , \quad \alpha_0 = \frac{6}{11 - 2N_F/C_A} \quad , \quad c_g = \frac{11}{6} \quad , \quad c_q = \frac{3}{2} \quad , \quad c_r = \frac{10}{27}\pi^2 - \frac{3}{2} \quad .$$

The constants  $c_q$  and  $c_g$  are corrections to the phase space available for the quark and gluon evolution,  $c_r$  determines a MLLA correction which is calculated with an estimated uncertainty of 10% and  $\Lambda$  is the QCD scale parameter. The solution of this differential equation implies a constant of integration. Extrapolating the solution of Eqn. 5 to small scales, neglecting the constant of integration, would imply that the multiplicity in a gg-system would still be significantly larger than in a  $q\bar{q}$ -system. At very small scales, however, the hadronic multiplicity of both systems should mainly be determined by hadronic phase space and thus should become almost equal [15]:

$$N_{gg}(L_0) \approx N_{q\bar{q}}(L_0) = N(L_0) \quad . \quad (6)$$

Thus a non-perturbative constant term appears in the solution for the gluon multiplicity as expected from the behaviour of the fragmentation functions. In [15] it is suggested to determine  $N(L_0)$  from data on charmonium or bottomium states.

The multiplicity of three-jet events is then given by the two alternative formulations [16]:

$$N_{q\bar{q}g} = N_{q\bar{q}}(L_{q\bar{q}}, \kappa_{Lu}) + \frac{1}{2} N_{gg}(\kappa_{Le}) \quad , \quad (7A)$$

$$N_{q\bar{q}g} = N_{q\bar{q}}(L, \kappa_{Lu}) + \frac{1}{2} N_{gg}(\kappa_{Lu}) \quad , \quad (7B)$$

henceforth referred to as predictions Eden A and Eden B, with

$$L = \ln \left( \frac{s}{\Lambda^2} \right) \quad , \quad L_{q\bar{q}} = \ln \left( \frac{s_{q\bar{q}}}{\Lambda^2} \right) \quad , \quad \kappa_{Lu} = \ln \left( \frac{p_{t,Lu}^2}{\Lambda^2} \right) \quad , \quad \kappa_{Le} = \ln \left( \frac{p_{t,Le}^2}{\Lambda^2} \right)$$

and

$$p_{t,Lu}^2 = \frac{s_{qg}s_{\bar{q}g}}{s} \quad , \quad p_{t,Le}^2 = \frac{s_{qg}s_{\bar{q}g}}{s_{q\bar{q}}} \quad , \quad s_{ij} = (p_i + p_j)^2 \quad .$$

The predictions Eqn. 7A and Eqn. 7B differ in the definition of the gluon contribution to the event multiplicity. In Eqn. 7A the  $q\bar{q}$ -contribution is determined mainly by the invariant mass of the  $q\bar{q}$ -system which is also the relevant scale in an  $q\bar{q}$ -event of the same topology with the gluon being replaced by a hard photon. In Eqn. 7B the  $q\bar{q}$ -contribution is given by the centre-of-mass energy of the whole event reflecting the phase-space available to the  $q\bar{q}$ -pair if no hard gluon had been emitted.

The expression  $N_{q\bar{q}}(L, \kappa)$  for the quark contribution to the three-jet multiplicity takes into account that the resolution of a gluon jet at a given  $p_t$  implies restrictions on the phase space of the quark system. This restricted multiplicity is linked to the multiplicity of an unrestricted  $q\bar{q}$ -system  $N_{q\bar{q}}(L)$  via [15]:

$$N_{q\bar{q}}(L, \kappa_{cut}) = N_{q\bar{q}}(\kappa_{cut} + c_q) + (L - \kappa_{cut} - c_q) \left. \frac{dN_{q\bar{q}}(L')}{dL'} \right|_{L'=\kappa_{cut}+c_q} \quad . \quad (8)$$

$N_F$	$a_1$	$a_2$	$a_3$
3	0.280	-0.379	0.209
4	0.297	-0.339	0.162
5	0.314	-0.301	0.112

Table 4: The coefficients  $a_i$  from [3]

$N_F$	$r_1$	$r_2$	$r_3$
3	0.185	0.426	0.189
4	0.191	0.468	0.080
5	0.198	0.510	-0.041

Table 5: The coefficients  $r_i$  from [3]

It is important to note that the unrestricted multiplicity is always a function of only one logarithmic energy scale, while the restricted multiplicity demands two logarithmic arguments. The equivalent restriction for the gluon contribution to the event multiplicity can be neglected, as the evolution scale of the gluon is the  $p_t$ -like variable  $\kappa$  and therefore coincides with the cut-off scale in Eqn. 8. Note also, that the topology dependence of the  $q\bar{q}$ -term in Eqn. 7B enters only due to this phase space restriction.

The explicit energy dependence of the multiplicity of unrestricted (“unbiased”)  $q\bar{q}$  events has already been calculated in [1]:

$$\langle N(Q^2) \rangle = a \cdot \alpha_s^b(Q^2) \cdot \exp\left(\frac{c}{\sqrt{\alpha_s(Q^2)}}\right) \cdot \left[1 + \mathcal{O}\left(\sqrt{\alpha_s(Q^2)}\right)\right] \quad (9)$$

with

$$b = \frac{1}{4} + \frac{2}{3} \frac{N_F}{\beta_0} \left(1 - \frac{C_F}{C_A}\right) \quad \text{and} \quad (10)$$

$$c = \sqrt{\frac{32\pi \cdot C_A}{\beta_0^2}} \quad . \quad (11)$$

In a more recent publication [3] the multiplicity of  $q\bar{q}$  or  $gg$  colour singlet systems has been calculated in 3NLO as an expansion of  $r$  and  $\gamma = \langle N_g \rangle' / \langle N_g \rangle$ , where the prime denotes a derivative with respect to the logarithmic energy scale  $y = \log(p\Theta/Q_0)$  with  $\Theta$  being the opening angle of the first splitting and  $Q_0$  the cut-off of the perturbative expansion. The mean multiplicities are then given by

$$\langle N_g(y) \rangle = k_g \cdot y^{-a_1 C^2} \cdot \exp[2C\sqrt{y} + \delta_g(y)] \quad (12)$$

and

$$\langle N_q(y) \rangle = \frac{k_q}{r_0} \cdot y^{-a_1 C^2} \cdot \exp[2C\sqrt{y} + \delta_q(y)] \quad . \quad (13)$$

$k_g$  and  $k_q$  denote free normalisations, the quantities  $r_i$  and  $a_i$  are calculated in [3] and given in Tab. 4 and Tab. 5,  $C = \sqrt{4N_C/\beta_0}$  and the additional contributions to the exponent are given as

$$\delta_g(y) = \frac{C}{\sqrt{y}} \left[2a_2 C^2 + \frac{\beta_1}{\beta_0^2} \{\log(2y) + 2\}\right] + \frac{C^2}{y} \left[a_3 C^2 - \frac{a_1 \beta_1}{\beta_0^2} \{\log(2y) + 1\}\right] \quad (14)$$

and

$$\delta_q(y) = \delta_g(y) + \frac{C}{\sqrt{y}} r_1 + \frac{C^2}{y} \left(r_2 + \frac{r_1^2}{2}\right) \quad . \quad (15)$$

Due to the definitions of the evolution variables, which are not symmetric with respect to quarks and gluons, the multiplicity of the two-gluon system is given in a slightly higher order than the multiplicity of the quark-antiquark system.

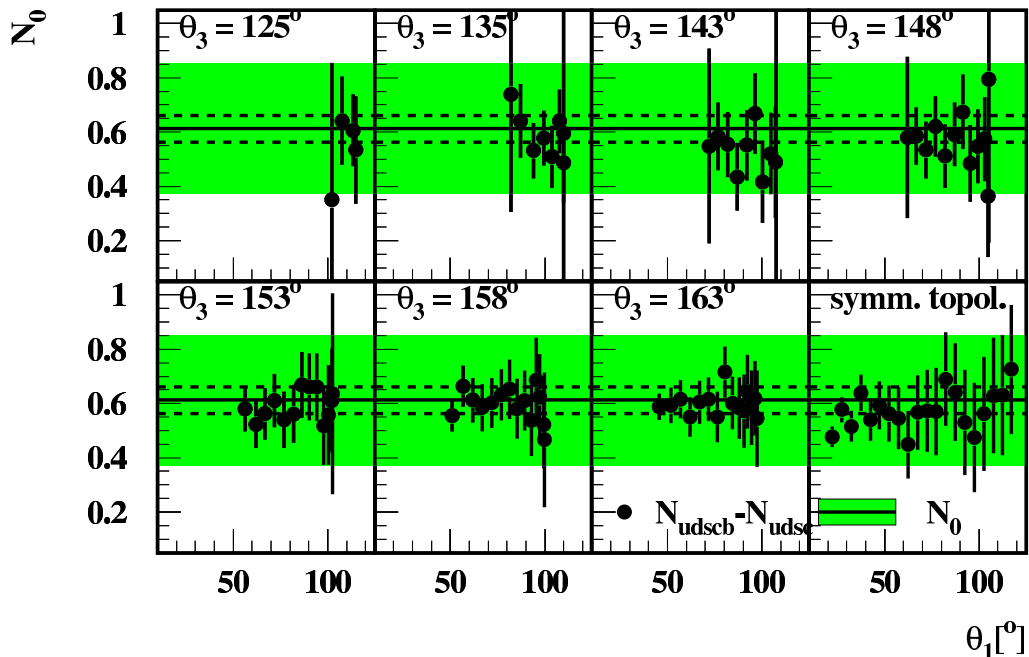


Figure 1: The multiplicity difference between  $udsc$ - and  $udscb$ -events. The shaded area reflects the value for  $N_0$  from Eqn. 19, the dashed lines indicate statistical errors only.

## 4 Mean multiplicity of hadronic events

The mean multiplicity of hadronic events at  $\sqrt{s} = m_Z$ , without consideration of the event topology, is found in this analysis to be  $20.963 \pm 0.004$  for  $udscb$ - and  $20.353 \pm 0.004$  for  $udsc$ -events with statistical errors only. The multiplicity of  $udscb$ -events is expected to be slightly larger than the multiplicity of  $udsc$ -events due to the additional multiplicity produced in  $B$  decays. These values are in good agreement with previous measurements of this quantity [4]. From this measurement the difference in multiplicity between  $udscb$ - and  $udsc$ -events, which proves to be crucial for this analysis, has been found to be

$$N_0 \equiv \delta_{udscb-udsc} = N_{udscb} - N_{udsc} = 0.610 \pm 0.002_{\text{stat}} \quad , \quad (16)$$

where the error of the difference has been determined assuming a correlation of  $\sqrt{1 - R_b} \sim 0.9$  between the two measurements.  $R_b$  denotes the fraction of hadronic events with initial  $b$ -quarks, which has been measured on the  $Z$  resonance [28]:

$$R_b(m_Z) = 0.21638 \pm 0.00066 \quad . \quad (17)$$

From previous measurements of the multiplicity of  $udscb$ - and  $b$ -events [29,30],  $N_0$  can be calculated using the relation

$$N_0 = 2 \frac{R_b}{1 - R_b} \cdot \left( \langle n_h \rangle_b - \langle n_h \rangle \right) \quad , \quad (18)$$

where  $\langle n_h \rangle_b$  and  $\langle n_h \rangle$  represent the multiplicity per hemisphere in a  $b$ - or a general hadronic event, respectively. The value obtained from the results in [29] is  $N_0 = 0.60 \pm 0.06$ , while the value obtained from the results in [30] is  $N_0 = 0.62 \pm 0.07$ , both in very good agreement with the value of this analysis. The given statistical errors are larger than the statistical error of  $N_0$  from this analysis, as in [29] and [30]  $N_b$  is measured

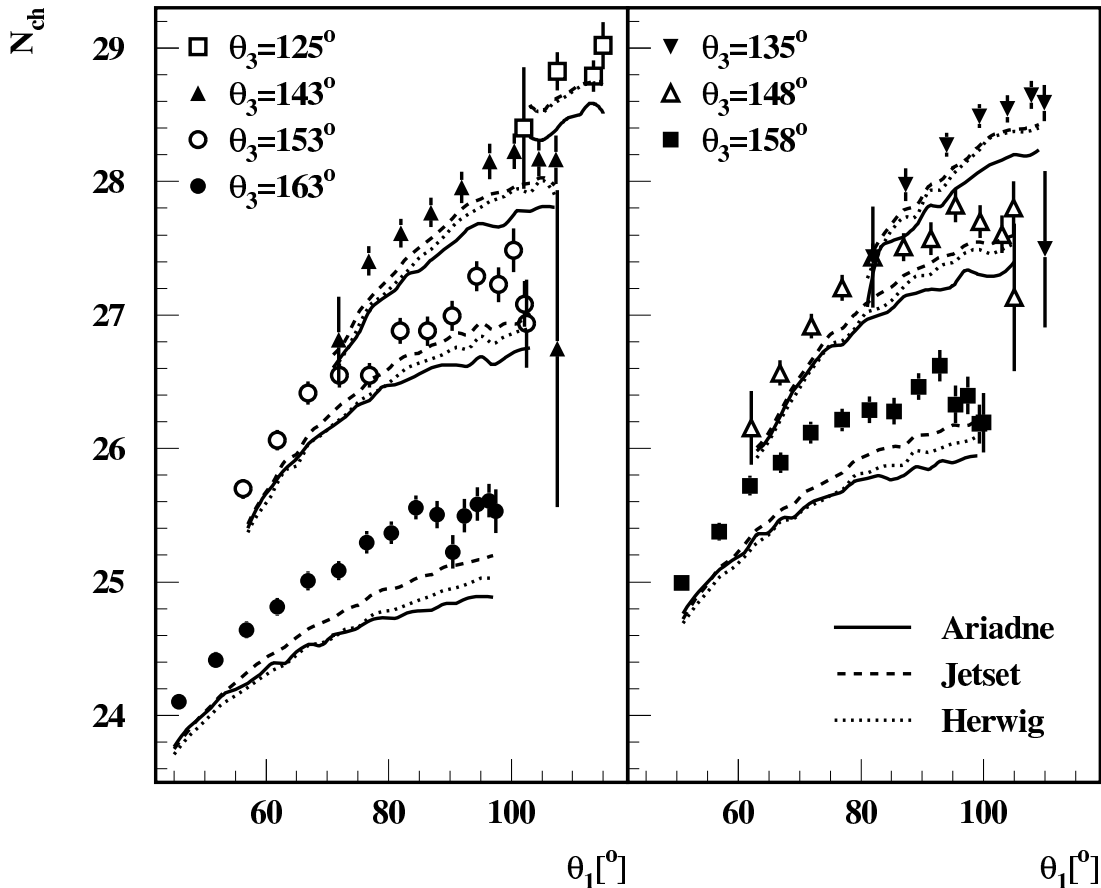


Figure 2: The mean charged multiplicity of  $udscb$ -events with general topologies as a function of the opening angle  $\theta_1$  for different values of  $\theta_3$  in comparison with the predictions of Monte Carlo models. The data points have been plotted in two diagrams with alternating  $\theta_3$ -bins, as the neighbouring curves would otherwise overlap. The errors shown are statistical only.

instead of  $N_{udsc}$ , so the determination of  $N_0$  is less direct and based on a smaller event sample. The systematic errors of  $N_b$  are  $\pm 0.22$  in [29] and  $\pm 0.24$  in [30]. The average of these two values for  $N_0$  is

$$N_0 = 0.61 \pm 0.24 \quad (19)$$

where also the given systematic errors on  $N_b$  have been considered.

The additional multiplicity due to initial  $b$ -quarks is in MLLA predicted to be independent of the centre-of-mass energy due to energy conservation and coherence effects in the gluon-radiation from heavy quarks [31]. This energy independence has been experimentally verified (see e.g. [32]). In Fig. 1 the multiplicity difference between  $udscb$ - and  $udsc$ -events  $N_0$  is shown as a function of the event topology. The shaded area reflects the value given in Eqn. 19, the dashed lines indicate the purely statistical error on  $N_0$ . No significant tendency can be observed,  $N_0$  can be considered as independent of the event topology within the angular regions studied.

The dependence of the multiplicity of  $udscb$ -events on the event topology is shown in Fig. 2 for general and in Fig. 3 for symmetric event topologies. For symmetric topologies a nearly logarithmic increase of multiplicity with increasing  $\theta_1$  can be observed. Also

$\vartheta_2$	$\vartheta_3$	$N_{\text{ch}}^{uds\text{cb}}$	$\vartheta_2$	$\vartheta_3$	$N_{\text{ch}}^{uds\text{cb}}$
99°	163°	25.53 ±0.16 ±0.12	121°	153°	26.88 ±0.11 ±0.06
101°	158°	26.19 ±0.22 ±0.14	121°	158°	26.29 ±0.10 ±0.02
101°	163°	25.61 ±0.12 ±0.06	121°	163°	25.30 ±0.08 ±0.05
103°	153°	26.94 ±0.33 ±0.11	126°	125°	28.83 ±0.15 ±0.12
103°	158°	26.18 ±0.15 ±0.10	126°	135°	28.49 ±0.09 ±0.09
103°	163°	25.58 ±0.12 ±0.10	126°	143°	27.96 ±0.12 ±0.09
105°	148°	27.13 ±0.55 ±0.42	126°	148°	27.51 ±0.10 ±0.06
105°	153°	27.08 ±0.17 ±0.09	126°	153°	26.88 ±0.10 ±0.05
105°	158°	26.40 ±0.14 ±0.09	126°	158°	26.21 ±0.09 ±0.04
105°	163°	25.49 ±0.13 ±0.11	126°	163°	25.08 ±0.07 ±0.02
107°	143°	26.75 ±1.19 ±0.79	131°	125°	28.40 ±0.46 ±0.22
107°	148°	27.80 ±0.20 ±0.13	131°	135°	28.28 ±0.09 ±0.07
107°	153°	27.49 ±0.16 ±0.07	131°	143°	27.77 ±0.11 ±0.05
107°	158°	26.33 ±0.14 ±0.07	131°	148°	27.43 ±0.10 ±0.08
107°	163°	25.23 ±0.12 ±0.05	131°	153°	26.55 ±0.09 ±0.08
110°	135°	27.49 ±0.59 ±0.35	131°	158°	26.12 ±0.08 ±0.04
110°	143°	28.16 ±0.18 ±0.12	131°	163°	25.01 ±0.07 ±0.07
110°	148°	27.60 ±0.14 ±0.08	136°	135°	27.98 ±0.12 ±0.07
110°	153°	27.23 ±0.13 ±0.04	136°	143°	27.61 ±0.11 ±0.08
110°	158°	26.62 ±0.12 ±0.06	136°	148°	27.20 ±0.10 ±0.06
110°	163°	25.50 ±0.10 ±0.09	136°	153°	26.55 ±0.09 ±0.06
113°	135°	28.59 ±0.13 ±0.06	136°	158°	25.89 ±0.08 ±0.08
113°	143°	28.17 ±0.13 ±0.09	136°	163°	24.81 ±0.07 ±0.07
113°	148°	27.70 ±0.12 ±0.11	141°	135°	27.43 ±0.38 ±0.24
113°	153°	27.29 ±0.11 ±0.07	141°	143°	27.41 ±0.11 ±0.07
113°	158°	26.46 ±0.10 ±0.05	141°	148°	26.92 ±0.09 ±0.09
113°	163°	25.56 ±0.09 ±0.09	141°	153°	26.41 ±0.09 ±0.06
117°	125°	29.02 ±0.18 ±0.12	141°	158°	25.72 ±0.07 ±0.05
117°	135°	28.65 ±0.10 ±0.06	141°	163°	24.64 ±0.06 ±0.05
117°	143°	28.23 ±0.13 ±0.06	146°	143°	26.81 ±0.32 ±0.31
117°	148°	27.82 ±0.12 ±0.07	146°	148°	26.56 ±0.09 ±0.07
117°	153°	26.99 ±0.11 ±0.06	146°	153°	26.06 ±0.08 ±0.09
117°	158°	26.28 ±0.10 ±0.03	146°	158°	25.38 ±0.07 ±0.07
117°	163°	25.37 ±0.09 ±0.05	146°	163°	24.41 ±0.06 ±0.07
121°	125°	28.79 ±0.12 ±0.08	152°	148°	26.16 ±0.28 ±0.14
121°	135°	28.54 ±0.10 ±0.10	152°	153°	25.70 ±0.07 ±0.07
121°	143°	28.15 ±0.13 ±0.08	152°	158°	24.99 ±0.05 ±0.08
121°	148°	27.57 ±0.12 ±0.08	152°	163°	24.10 ±0.04 ±0.08

Table 6: The multiplicity of  $uds\text{cb}$ -events in dependence of the event topology for general topologies. The values for  $\theta_2$  and  $\theta_3$  represent the centre of the bins, not averages, i.e. due to bin overlap it can happen that the given value for  $\theta_2$  is larger than the corresponding value for  $\theta_3$ . The first errors are statistical, the second errors are systematic errors due to the choice of the cluster algorithm and variations of track and event cuts.

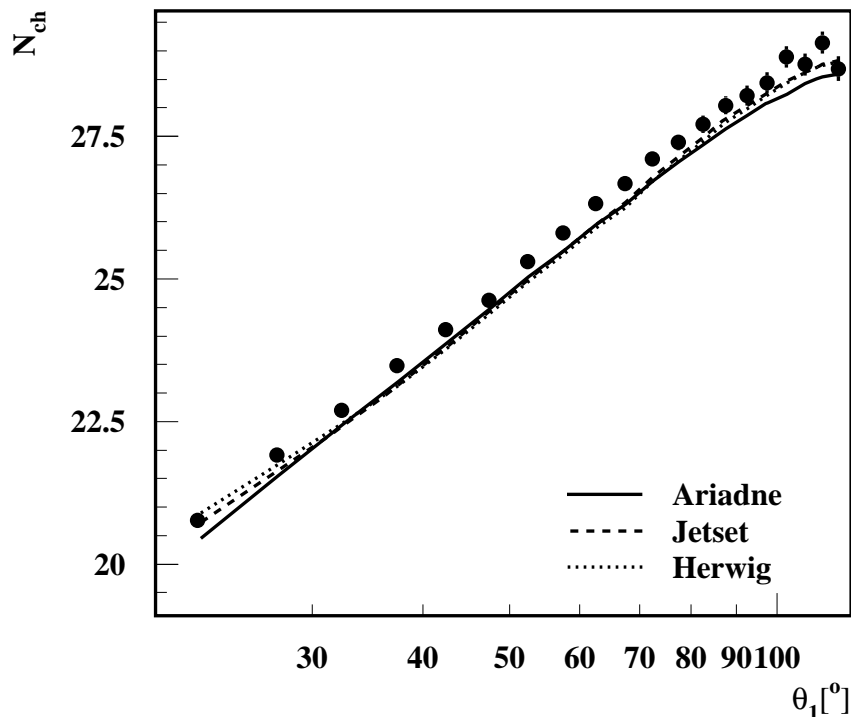


Figure 3: The mean charged multiplicity of  $udscb$ -events with symmetric topology as a function of the opening angle  $\theta_1$  in comparison with the predictions of Monte Carlo models. The errors shown are statistical only.

for general topologies the event multiplicity increases with  $\theta_1$  for a fixed value of  $\theta_3$ . For general event topologies also an increase of multiplicity with decreasing  $\theta_3$  can be observed. This dependence is more pronounced than the  $\theta_1$ -dependence as a change in  $\theta_1$  of  $50^\circ$  results in a multiplicity change of roughly 2 units, while the same change in  $\theta_3$  leads to a change in multiplicity of roughly 4 units. The Monte Carlo models, although mutually agreeing well, underestimate the multiplicity by  $\sim 0.4$  units. In Fig. 2 it can be seen that the deviation is stronger for large values of  $\theta_3$  than for smaller values.

## 5 Preparation of the prediction

Eqn. 7A and Eqn. 7B give the average multiplicity of a three-jet event in terms of the restricted  $q\bar{q}$ -multiplicity and the multiplicity of a two-gluon system. Both contributions can be derived from the unrestricted  $q\bar{q}$ -multiplicity using Eqn. 8 and Eqn. 5, which has been measured in numerous  $e^+e^-$  experiments at different centre-of-mass energies. The aim of this section is to provide a closed parametrisation of  $N_{q\bar{q}g}$  using a parametrisation of the measured unrestricted multiplicity  $N_{q\bar{q}}(\sqrt{s})$ .

The measurements of  $N_{q\bar{q}}(\sqrt{s})$  used [4] are shown in the central part of Fig. 4. Not included are older measurements of the JADE and PLUTO collaboration in which the pions from the decay  $K^0 \rightarrow \pi\pi$  have not been added to the multiplicity [33]. Recent results of a re-analysis of the JADE data [34] are, taken into account. In these measurements events with initial  $b$ -quarks are included. Due to the decay products of the  $b$ -containing mesons these events have an increased multiplicity. As the fraction of events with initial

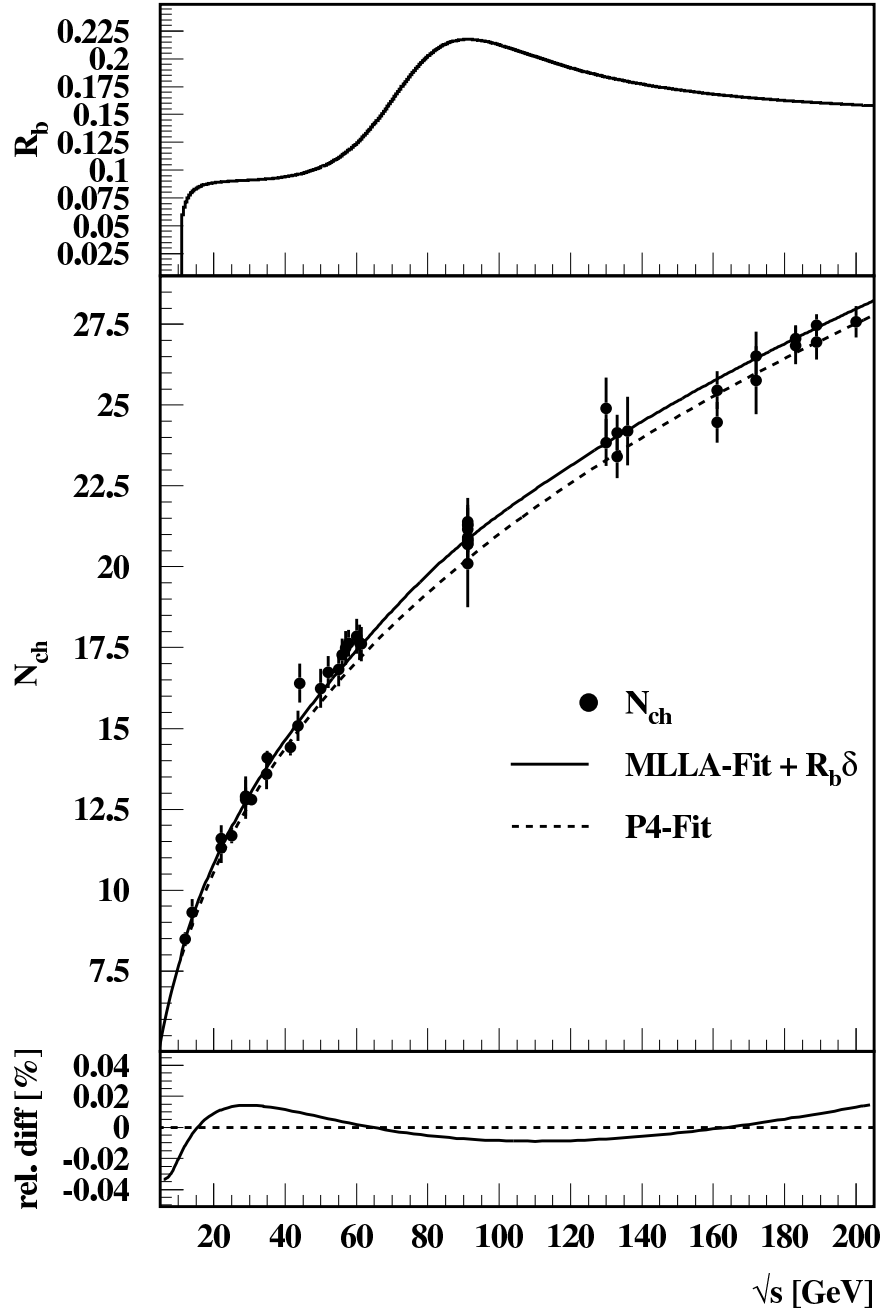


Figure 4: **Top:** The branching ratio  $R_b$  as a function of  $\sqrt{s}$ . **Middle:** The measurements of  $N_{q\bar{q}}$  [4,5] with the fitted parametrisation Eqn. 22. Note that the 4th order polynomial P4 fit does not account for the additional multiplicity due to  $b$ -events. **Bottom:** The relative deviation of the fitted polynomial P4 from the parametrisation Eqn. 9

$\vartheta_1$	$N_{\text{ch}}^{udscb}$	$\vartheta_1$	$N_{\text{ch}}^{udscb}$
22°	20.77 ±0.03 ±0.24	72°	27.11 ±0.13 ±0.10
27°	21.91 ±0.04 ±0.18	77°	27.40 ±0.14 ±0.08
32°	22.70 ±0.05 ±0.13	82°	27.71 ±0.15 ±0.11
37°	23.48 ±0.06 ±0.10	87°	28.05 ±0.16 ±0.06
42°	24.11 ±0.07 ±0.09	92°	28.21 ±0.17 ±0.13
47°	24.63 ±0.08 ±0.09	97°	28.44 ±0.18 ±0.10
52°	25.30 ±0.09 ±0.06	102°	28.89 ±0.19 ±0.14
57°	25.81 ±0.10 ±0.08	107°	28.76 ±0.19 ±0.07
62°	26.32 ±0.11 ±0.10	112°	29.14 ±0.20 ±0.07
67°	26.67 ±0.12 ±0.05	117°	28.68 ±0.22 ±0.14

Table 7: The multiplicity of  $udscb$ -events in dependence of the event topology for symmetric topologies. The first errors are statistical, the second errors are systematic errors due to the choice of the cluster algorithm and variations of track and event cuts.

$b$ -quarks varies with the centre-of-mass energy, this additional multiplicity introduces an additional energy dependence of the multiplicity which is not due to strong interactions and which has to be corrected for. The upper plot of Fig. 4 shows the branching ratio

$$R_b = \frac{\sigma(e^+e^- \rightarrow b\bar{b})}{\sigma(e^+e^- \rightarrow \text{hadrons})} \quad (20)$$

as a function of the centre-of-mass energy. The curve has been obtained using the LUX-TOT routine of the JETSET/PYTHIA package [24]. The average additional multiplicity due to  $b$ -events can be expressed in terms of  $N_0$ :

$$\delta_{b-udsc} = 2 \cdot \left( \langle n_h \rangle_b - \langle n_h \rangle_{udsc} \right) = \frac{N_0}{R_b(m_Z)} \quad (21)$$

With the values from Eqn. 17 and Eqn. 19, the multiplicity difference can be determined giving  $\delta_{b-udsc} = 2.83 \pm 0.23$ .

The  $q\bar{q}$ -multiplicities are then fitted with the function

$$N_{udscb}(\sqrt{s}) = N_{udsc}(\sqrt{s}) + \delta_{b-udsc} \cdot R_b(\sqrt{s}) \quad (22)$$

where Eqn. 9 is used to parametrise  $N_{udsc}(\sqrt{s})$ . The description of the data is very good with a  $\chi^2$  per degree of freedom of 33/48. The values found for the fit parameters are

$$a = 0.10252 \pm 0.0025$$

$$\Lambda = (0.243 \pm 0.012) \text{ GeV} \quad .$$

The fitted function is indicated in Fig. 4 as a solid line. To simplify the integration of  $N_{udsc}(\sqrt{s})$  required due to Eqn. 5, a polynomial of order four in  $L = \log(s/\Lambda^2)$  is fitted to the parametrisation of  $N_{udsc}(\sqrt{s})$ . The fit is performed with  $\Lambda = 0.25$  GeV, and the values obtained for the coefficients are given in Tab. 8. The polynomial is indicated as a dashed line in the middle plot of Fig. 4. The difference between the dashed polynomial and the solid line indication of Eqn. 22 is due to the omission of the  $\delta_{b-udsc} \cdot R_b(\sqrt{s})$  term. In the lower part of Fig. 4 the relative deviation of the polynomial from the fitted  $N_{udsc}(\sqrt{s})$  is shown. The deviations are smaller than  $2 \cdot 10^{-4}$  over most of the fitted region and nowhere exceed  $4 \cdot 10^{-4}$ , indicating an excellent description of  $N_{udsc}(\sqrt{s})$  by



$p_0$	0.18981
$p_1$	0.40950
$p_2$	$0.57358 \cdot 10^{-1}$
$p_3$	$0.10349 \cdot 10^{-2}$
$p_4$	$0.28640 \cdot 10^{-3}$

Table 8: The coefficients of the polynomial fitted to  $N_{ch}^{udsc}(\sqrt{s})$

the polynomial. The value of the polynomial at  $\sqrt{s} = m_Z$  is 20.2561. This value is in good agreement with the mean multiplicity of  $udsc$ -events of  $20.353 \pm 0.004$  measured in this analysis. The small difference is taken into account when considering the systematic errors of this analysis.

Inserting the polynomial into Eqn. 5 and Eqn. 8 leads to a closed form of the predictions of Eqn. 7A and Eqn. 7B. To fix the constant of integration, left free in Eqn. 5, a measurement of  $N_{gg}$  from  $\chi'$  decays by the CLEO collaboration is used [35]. The value of  $N_{gg}(9.9132 \text{ GeV}) = 9.339 \pm 0.090 \pm 0.045$  using  $\Lambda = 250 \text{ MeV}$  results in  $L_0 = 5.86$ , which corresponds to a centre-of-mass energy of 4.68 GeV at which quark and gluon multiplicities are equal.

Assuming massless jet kinematics, the scale variables  $\kappa_{Lu}$ ,  $\kappa_{Le}$  and  $L_{q\bar{q}}$  can directly be expressed only in terms of the inter-jet angles  $\theta_i$  (and the constant centre-of-mass energy). This yields  $N_{q\bar{q}g}$  as a function of the inter-jet angles under the assumption that a certain jet is the gluon jet. As no explicit identification of the gluon jet is made,  $N_{q\bar{q}g}$  is calculated for all three possible gluon jet hypotheses and the weighted mean of these values is taken, where each hypothesis is weighted with the corresponding value of the three-jet matrix-element which can be calculated from the inter-jet angles assuming again massless jet kinematics.

However, it is a known feature of the hadronisation process that due to coherent production of inter-jet particles close-by jets are pulled even closer together. The calculations leading to Eqn. 7A and Eqn. 7B refer to the partonic structure of an event. While for the change in multiplicity due to the hadronisation process in accordance with the LPHD hypothesis an overall normalisation constant can be found, for the change in the event topology, i.e. the inter-jet angles, this is not the case. Therefore, a topology dependent hadronisation correction has to be applied. The effect can be most easily understood for symmetric event topologies. During the hadronisation process jets two and three are pulled closer together resulting in a smaller opening angle  $\theta_1$  at the hadronic than at the partonic level of the event. As the multiplicity increases with  $\theta_1$ , the reduced  $\theta_1$  found at the hadronic level thus results in an underestimation of the multiplicity compared to the prediction which is based on the value of  $\theta_1$  at parton level.

This effect is corrected for by a topology dependent correction factor which is applied to the prediction. In Fig. 5 the correction factors obtained for symmetric event topologies are shown. The correction factors are calculated by dividing the mean hadron multiplicity obtained for a certain  $\theta_1$  bin (with  $\theta_1$  measured at the hadronic level of the simulated event) by the mean hadron multiplicity obtained with  $\theta_1$  measured at the partonic level of the event. The correction factors shown are taken from the ARIADNE Monte Carlo simulation for each of the four cluster algorithms used. The correction factor is around unity for large opening angles and increases for small  $\theta_1$ . This follows the expectation that jets which are close together are pulled even closer together than jets with a larger

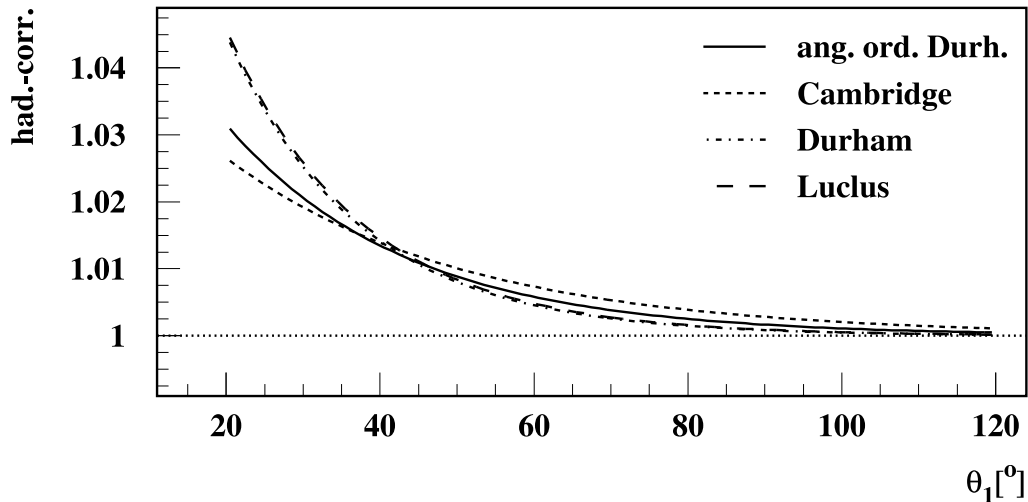


Figure 5: The hadronisation correction factor for symmetric topologies from the ARIADNE Monte Carlo. Plotted is the ratio of multiplicities with  $\theta_1$  determined at the hadronic level and the multiplicities with  $\theta_1$  determined at the partonic level.

		a.o.D.	Camb.	Durh.	Lucl.
ARIADNE	$a_1$	-0.0417134	-0.0317331	-0.0564096	-0.0554275
	$a_2$	0.07052	0.0487817	0.133435	0.132929
JETSET	$a_1$	-0.0591038	-0.0455694	-0.0750201	-0.0564708
	$a_2$	0.111077	0.0804121	0.240021	0.149093
HERWIG	$a_1$	-0.0843598	-0.147902	-0.0788673	-0.0680853
	$a_2$	0.549409	0.869146	0.727511	0.521014

Table 9: The parameters of the hadronisation correction factors for symmetric event topologies

angle between them. In order to get a smooth correction the function

$$c = \frac{1}{1 - a_2 e^{a_1 \theta_1}} \quad (23)$$

is fitted to the correction factors. The correction is described very well by the fitted function, the corrections obtained for the four studied cluster algorithms are shown in Fig. 5. The fitted parameters obtained using the Monte Carlo generators ARIADNE, HERWIG and JETSET are given in Tab. 9 for the four cluster algorithms. The same procedure is applied also to events with general topologies. In Fig. 6 the correction factors obtained with ARIADNE for the four used cluster algorithms are shown for several values of  $\theta_3$  as a function of  $\theta_1$ . In order to describe these corrections smoothly the two-dimensional function

$$c = (a_1 + a_2 \theta_3 + a_5 \theta_3^2) + (a_3 + a_4 \theta_3 + a_6 \theta_3^2) \cdot \theta_1 \quad (24)$$

is fitted to the correction factors. The description of the correction by the fit is reasonable, and the parameter values obtained are listed in Tab. 10. In general, the correction becomes smaller with increasing opening angle  $\theta_1$ , as expected for this hadronisation effect.

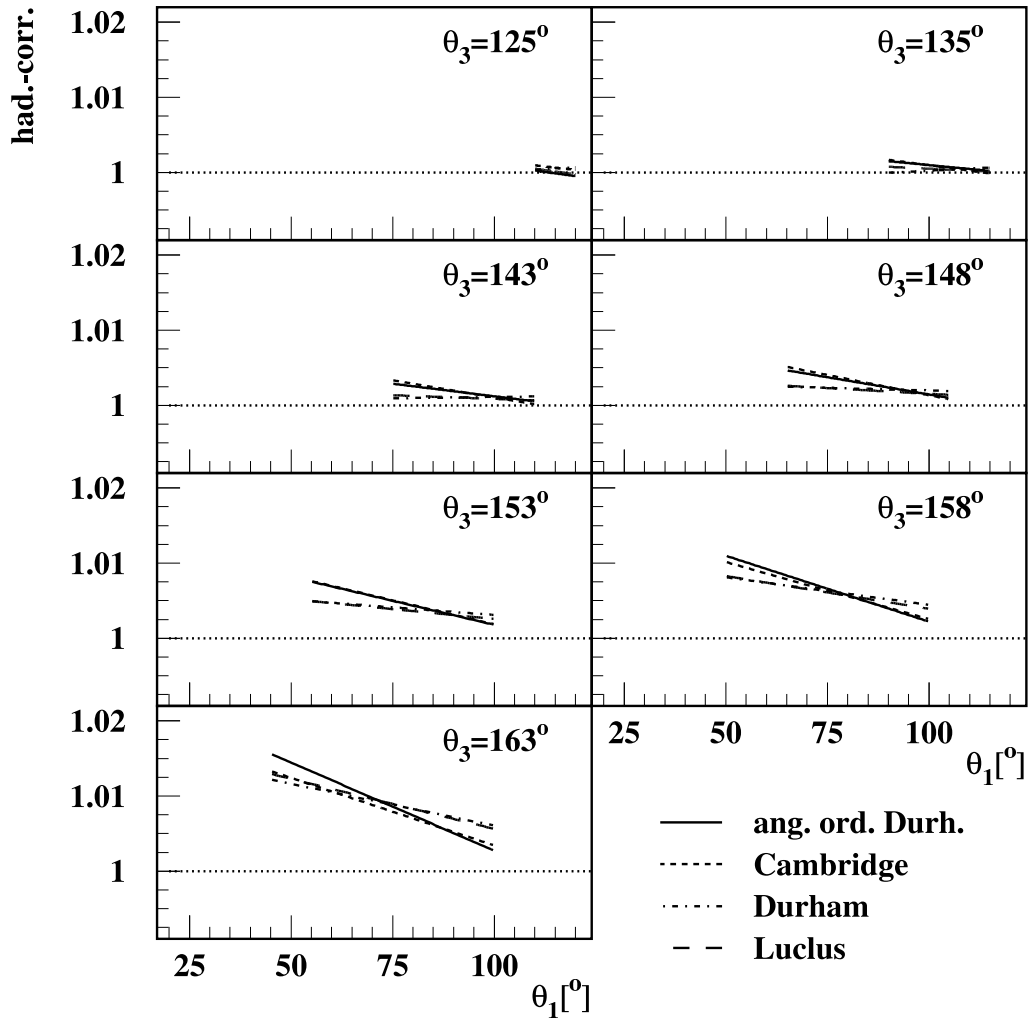


Figure 6: The hadronisation correction factors for general topologies. Plotted is the ratio of multiplicities with the inter-jet angles determined at the hadronic level over the multiplicities with the inter-jet angles determined at the partonic level.

		a.o.D.	Camb.	Durh.	Lucl.
ARIADNE	$a_1$	1.45743	1.19004	1.26382	1.58878
	$a_2 \cdot 10^3$	-6.7041	-2.85481	-4.1925	-8.40213
	$a_3 \cdot 10^3$	-4.27398	-1.15495	-1.83942	-4.62464
	$a_4 \cdot 10^5$	6.25913	1.78559	2.94159	6.54661
	$a_5 \cdot 10^5$	2.48986	1.11675	1.64381	3.00994
	$a_6 \cdot 10^7$	-2.31969	-0.728499	-1.15423	-2.32587
JETSET	$a_1$	0.925643	1.34605	1.47339	1.33754
	$a_2 \cdot 10^3$	0.604669	-4.93063	-6.55149	-4.90623
	$a_3 \cdot 10^3$	1.5079	-2.33696	-3.10136	-2.0464
	$a_4 \cdot 10^5$	-1.75222	3.32752	4.17083	2.84691
	$a_5 \cdot 10^5$	-0.019105	1.80813	2.29184	1.81215
	$a_6 \cdot 10^7$	0.449687	-1.23386	-1.42457	-1.01679
HERWIG	$a_1$	0.910054	1.22464	1.41922	0.820707
	$a_2 \cdot 10^3$	0.994144	-3.11472	-6.18148	1.78567
	$a_3 \cdot 10^3$	2.14597	-0.3132	-2.81892	2.43204
	$a_4 \cdot 10^5$	-2.94057	0.232189	4.03189	-3.00669
	$a_5 \cdot 10^5$	-0.208228	1.12039	2.28406	-0.351293
	$a_6 \cdot 10^7$	0.947642	-0.0622476	-1.46606	0.888795

Table 10: The parameters for the hadronisation correction factors for general topologies for the angular ordered Durham (a.o.D.), Cambridge (Camb.), Durham (Durh.) and Luclus (Lucl.) algorithm

## 6 The fit of $C_A/C_F$

The closed form of  $N_{q\bar{q}g}$  as a function of the event topology obtained from Eqn. 7A (Eden A) and Eqn. 7B (Eden B) with the procedure described in Sect. 5 can now be compared with the measured three-jet event multiplicities. In Fig. 7 the measured multiplicities of  $udsc$ - (open markers) and  $udscb$ -events (solid markers) are shown for symmetric and general topologies. The two solid lines indicate the respective predictions of Eqn. 7A where for  $udscb$ -events the constant  $N_0$  of Eqn. 19 has been added to the prediction. The dashed lines represent the respective predictions of Eqn. 7B. It can be observed that prediction Eqn. 7A describes the multiplicity of symmetric events in an excellent way, while Eqn. 7B overestimates the multiplicity by  $\sim 0.6$ , with the result that the prediction for  $udsc$ -events almost coincides with the multiplicities measured in  $udscb$ -events. Moreover, the slope of Eqn. 7B seems to be larger than the slope of the measured multiplicities. For general topologies an overall good description of the event multiplicities by Eqn. 7A can be seen. Only for large  $\theta_3$  and then especially for large  $\theta_1$ , i.e. in topologies where jet 3 is not strongly pronounced, larger deviations occur. Again, Eqn. 7B overestimates the multiplicities significantly and shows a larger slope with respect to  $\theta_1$ .

In order to determine the colour factor ratio  $C_A/C_F$  from the event multiplicities, the predictions Eqn. 7A and Eqn. 7B are fitted to the data. To avoid systematic uncertainties entering through the use of a  $b$ -tagging procedure,  $udscb$ -events are used to obtain the central result, while the results obtained for  $udsc$ -events are considered when estimating systematic uncertainties.  $C_A/C_F$  enters the prediction only via the *derivative* of the gluon multiplicity in Eqn. 5, so this parameter is expected to be sensitive to the change

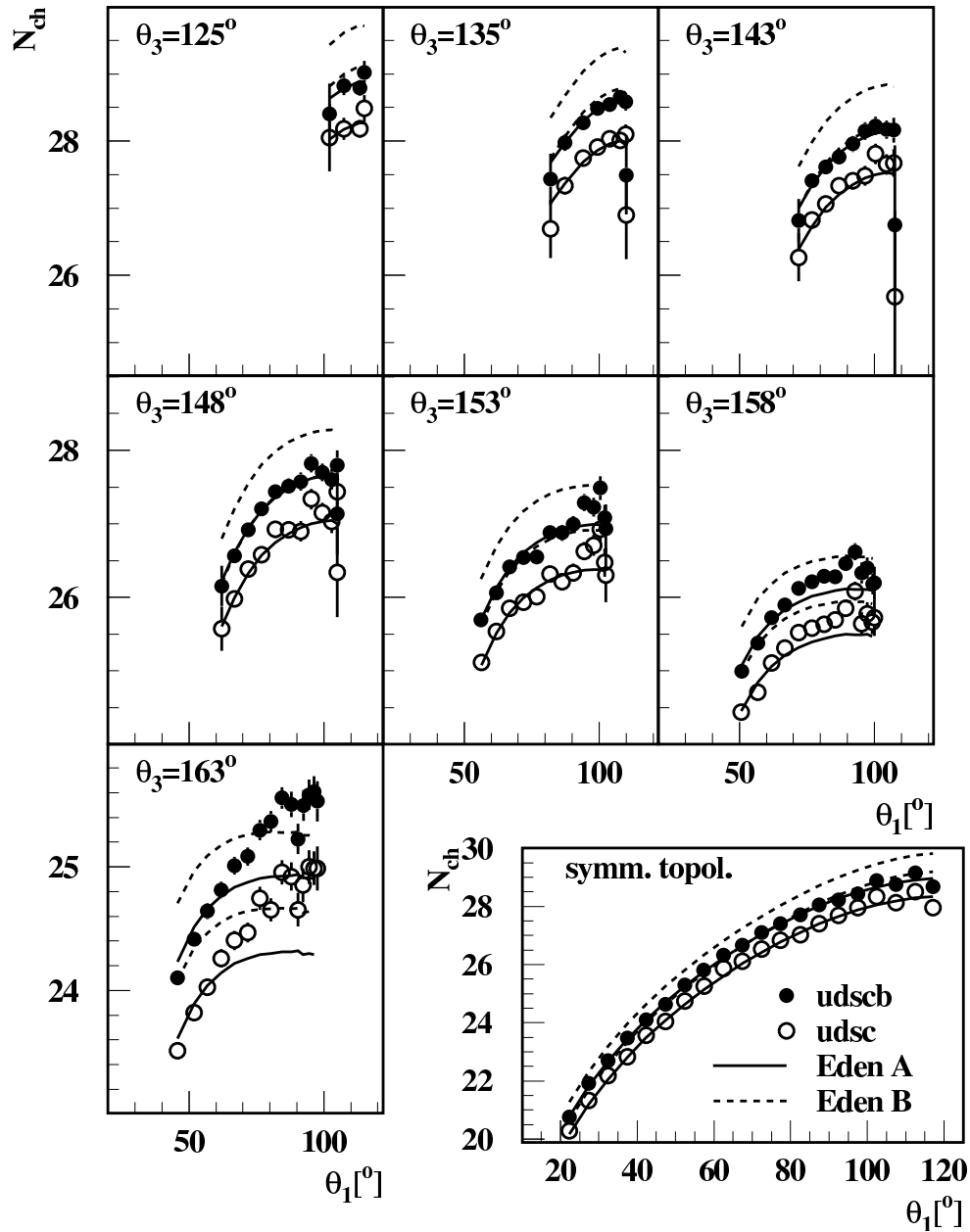


Figure 7: The mean multiplicity of *udschb*- and *udsc*-events with symmetric and general topologies in comparison with the predictions Eqn. 7A and Eqn. 7B prepared as described in Sect. 5. The error bars indicate statistical errors only.

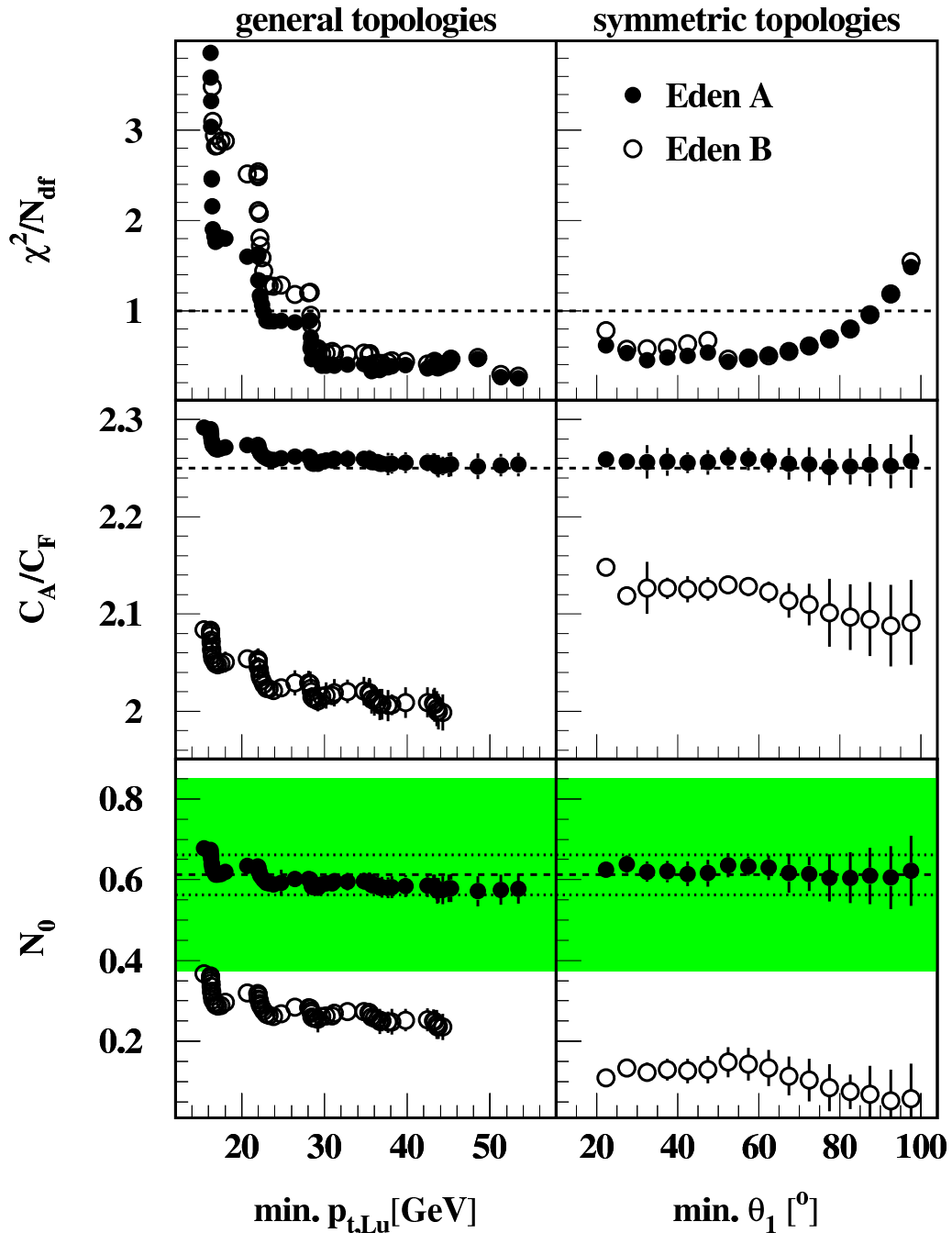


Figure 8: The fit parameters  $\chi^2/N_{df}$ ,  $C_A/C_F$  and  $N_0$  as function of the fit range. The shaded area indicates the expected value of  $N_0$  with statistical and systematic uncertainties, the dotted lines indicate statistical errors only. The dashed lines indicate 1.0 in the top,  $C_A/C_F = 2.25$  in the middle and the  $N_0$  value from Eqn. 19 in the bottom plots.

		Eden A		Eden B	
		$C_A/C_F$	$N_0$	$C_A/C_F$	$N_0$
<i>udscb</i>	symm.	$2.257\pm 0.019$	$0.62\pm 0.03$	$2.127\pm 0.034$	$0.12\pm 0.03$
	gen.	$2.261\pm 0.014$	$0.60\pm 0.03$	$2.028\pm 0.050$	$0.28\pm 0.03$
<i>udsc</i>	symm	$2.237\pm 0.030$	$0.09\pm 0.05$	$2.101\pm 0.096$	$-0.42\pm 0.13$
	gen.	$2.272\pm 0.015$	$0.01\pm 0.04$	$2.039\pm 0.056$	$-0.30\pm 0.08$

Table 11: The results of the parameter fit for  $C_A/C_F$  and  $N_0$

of multiplicity rather than to its absolute value. Therefore, the additional constant  $N_0$  is allowed to vary freely in the fit (also when fitting *udsc*-events where  $N_0$  is expected to be zero) in order to avoid an influence of the absolute value on the fit result for  $C_A/C_F$ .

The fit range used is determined by the value of  $\chi^2/N_{df}$  obtained with the fit. While for symmetric event topologies it is straightforward to determine the data points used in the fit by demanding a minimum opening angle  $\theta_1$ , the situation is not as clear for the general event topologies, where two variables are needed to describe a topology. A reasonable order criterium is a ‘three-jet likeliness’ of a topology, i.e. the emphasis which is put on the third jet. Therefore the  $p_t$  of the third jet is a reasonable ordering variable. It turned out that  $p_{t,Lu}$  is the best suited of the used  $p_t$ -like variables, because the fits converge fastest, if the fit range is determined by  $p_{t,Lu}$ . The fit range is then defined by demanding a minimum  $p_{t,Lu}$ -value for the event topologies used.

In the upper plots of Fig. 8 the values obtained for  $\chi^2/N_{df}$  when fitting *udscb*-events with the predictions of Eqn. 7A and Eqn. 7B are shown for both general and symmetric topologies. The values of  $\chi^2/N_{df}$  obtained for symmetric events are always smaller than 1.0, regardless of the chosen minimal  $\theta_1$ -value except for extremely small fit-ranges. The curves show a shallow minimum around  $\theta_1^{\min} \sim 30^\circ$  which is chosen to determine the fit-range. For general topologies, and a small minimal  $p_{t,Lu}$ , the  $\chi^2/N_{df}$  values are large but decrease fast with a more restricted fit range. The  $\chi^2/N_{df}$  curve shows a step-like structure, where every step corresponds to a completely excluded bin in  $\theta_3$ . From a minimum  $p_{t,Lu}$  value of  $\sim 22$  GeV on a plateau in the vicinity of  $\chi^2/N_{df} = 1$  can be observed and a minimum  $p_{t,Lu}$  of 25 GeV is chosen.

Fitting the data within these ranges results in the parameter values given in Tab. 11. As can be seen, the prediction of Eqn. 7A results in compatible values for  $C_A/C_F$  when fitting *udsc*- and *udscb*-events of symmetric or general topologies. Both values for  $N_0$  obtained by fitting *udscb*-events agree with the expectation of  $N_0 = 0.61$  as well as both  $N_0$  values for *udsc*-events agree with the expectation of  $N_0 = 0$ . The results obtained for  $C_A/C_F$  and  $N_0$  with Eqn. 7B in symmetric topologies are not in good agreement with the values obtained in general topologies. Also the values for  $N_0$  are not in agreement with the respective expectations. In the lower plots of Fig. 8 the fit results for  $C_A/C_F$  and  $N_0$  are shown for *udscb*-events as a function of the fit range. The parameters are correlated, but as this plot is only to show the influence of the fit range, when plotting the dependence of one parameter the other parameter is fixed to the respective value of Tab. 11. While Eqn. 7A leads to results which are independent of the fit range, the results of Eqn. 7B exhibit a more pronounced dependence on the fit range. Again, the discrepancy of the results obtained with Eqn. 7B for symmetric and general topologies can be observed, as well as the disagreement of the obtained values for  $N_0$  with the expectation indicated by the shaded area while fixing  $N_0$  to the expected values leads to an unacceptably high  $\chi^2/N_{df}$ .

variable	tight	loose
$p$	$\geq 0.5 \text{ GeV}$	$\geq 0.3 \text{ GeV}$
$\vartheta_{\text{polar}}$	$30^\circ - 150^\circ$	$20^\circ - 160^\circ$
$\epsilon_{xy}$	$\leq 2 \text{ cm}$	$\leq 8 \text{ cm}$
$\epsilon_z$	$\leq 8 \text{ cm}$	$\leq 12 \text{ cm}$
$\Delta p/p$	$\leq 80\%$	$\leq 120\%$

Table 12: Variations of the track cuts given in Tab. 1 for systematic studies

variable	tight	loose
general events		
$E_{\text{charged}}^{\text{hemisph.}}$	$\geq 0.05 \cdot \sqrt{s}$	$\geq 0.02 \cdot \sqrt{s}$
$E_{\text{charged}}^{\text{total}}$	$\geq 0.18 \cdot \sqrt{s}$	$\geq 0.06 \cdot \sqrt{s}$
$N_{\text{charged}}$	$\geq 6$	$\geq 4$
$\vartheta_{\text{sphericity}}$	$40^\circ - 140^\circ$	$30^\circ - 150^\circ$
$p_{\text{max}}$	20 GeV	70 GeV
three-jet events		
$\sum_{i=1}^3 \theta_i$	$> 357.5^\circ$	$> 350^\circ$
$E_{\text{visible}}/\text{jet}$	$\geq 8 \text{ GeV}$	$\geq 3 \text{ GeV}$
$\vartheta_{\text{jet}}$	$40^\circ - 140^\circ$	$30^\circ - 150^\circ$

Table 13: Variation of the event cuts given in Tab. 2 for systematic studies

Since the prediction Eqn. 7B, which depicts a rather extreme scenario of the phase-space assignment to quark and gluon jets, fails to give consistent results for symmetric and general topologies and because Eqn. 7B overestimates the event multiplicity in general which results in unphysically low values of  $N_0$ , this formulation of the prediction is discarded in favour of Eqn. 7A for the central result. The central results of the fits are therefore

$$\frac{C_A}{C_F} = 2.257 \pm 0.019_{\text{stat.}} \quad (25)$$

for symmetric and

$$\frac{C_A}{C_F} = 2.261 \pm 0.014_{\text{stat.}} \quad (26)$$

for general event topologies.

Several sources of systematic uncertainties have been considered. The systematic error on  $C_A/C_F$  is estimated by fitting prediction Eqn. 7A with the variations to the analysis listed below. As the parameters  $C_A/C_F$  and  $N_0$  are correlated and this correlation should not be reflected by the estimated systematic uncertainties,  $N_0$  is fixed at 0.61. The values obtained for  $C_A/C_F$  with the variations of the analysis are then compared to the result obtained by the standard analysis but with  $N_0$  fixed at the above value.

The studied experimental sources of uncertainty are:

- Variations of the track cuts listed in Tab. 1 within the ranges given in Tab. 12. The minimal track length is not lowered in order to maintain a contribution of the TPC detector to the track reconstruction;
- Variations of the cuts on the event- and jet-structure listed in Tab. 2 within the ranges given in Tab. 13 ;
- The hadronisation corrections are calculated from JETSET instead of ARIADNE simulation. Alternatively 30% of the hadronisation correction are regarded as this correction's uncertainty;
- Alternatively to the arithmetic mean of the multiplicity distributions, the mean multiplicities are determined by parameter fits of negative binomials to the distributions. As a further alternative, the matrix correction is replaced by a multiplicative correction to the mean multiplicities;
- The  $udsc$  sample is used to estimate the uncertainty of  $C_A/C_F$  due to the  $b$ -quark multiplicity;



		symm. topol.			general topol.		
exper- imental	track cuts	1.2%			0.4%		
	event cuts	0.8%			0.6%		
	hadr.-corr.	1.2%			0.4%		
	acc.-corr.	0.4%			0.2%		
	$udsc$ - / $udscb$ -sample	1.0%	2.5%		0.8%	1.6%	
	fit range	0.1%			0.0%		
	normalisation of $N_{q\bar{q}}$	0.5%		4.0%	0.5%		3.3%
	$e^+e^-$ fitted data	0.9%			0.7%		
variation of $\delta_{b-udsc}$	0.8%			0.7%			
theo- retical	variation of $\Lambda$	1.0%			1.0%		
	variation of $c_r$	2.0%	3.1%		2.1%	2.9%	
	variation of $L_0$	0.0%			0.0%		
	clustering algorithm	2.2%			1.8%		

Table 14: The relative systematic uncertainties of the measurement of  $C_A/C_F$ 

- The lower limit of the fit range is varied between  $\theta_1 > 25^\circ$  and  $\theta_1 > 35^\circ$  for symmetric events and between  $p_{t,\text{Lu}} > 22.5$  GeV and  $p_{t,\text{Lu}} > 28$  GeV for general topologies;
- The difference between the parametrisation of  $N_{q\bar{q}}$  at  $\sqrt{s} = m_Z$  and the event multiplicity measured in this analysis is 0.101 units, i.e. 0.5%. In the worst case this reflects an uncertainty on the normalisation of  $N_{q\bar{q}}$  which would directly be reflected in  $C_A/C_F$ . Therefore this deviation is considered conservatively as the relative uncertainty on  $C_A/C_F$ ;
- The data set used to fit the parametrisation of  $N_{q\bar{q}}$  is varied, by excluding the results of the TOPAZ, JADE and MARK-I collaborations or the results of the AMY collaboration respectively;
- The correction due to the additional multiplicity in  $b$ -events is varied within the errors of  $\delta_{b-udsc}$  when fitting the parametrisation of  $N_{q\bar{q}}$ .

Additionally, the uncertainty due to the choice of the clustering algorithm has been estimated by comparing the result obtained with the angular ordered Durham algorithm with the results obtained using the Durham, Cambridge and Luclus algorithms. Moreover the following uncertainties of the theoretical prediction have been studied:

- The scale variable  $\Lambda$  has been varied between 200 MeV and 300 MeV;
- The constant  $c_r$  has been varied within the given theoretical uncertainty of  $\sim 10\%$ ;
- The measurement of  $N_{gg}$  by CLEO which has been used to determine  $L_0$  has been varied within the given errors. As  $L_0$  is a constant of integration it is supposed to affect mainly  $N_0$  and not  $C_A/C_F$ . Therefore  $N_0$  is varied freely when estimating the effect of variations of  $L_0$ . Indeed no dependence of  $C_A/C_F$  on the variation of  $L_0$  is observed.

The relative uncertainties caused by the different sources are given in Tab. 14. Alternatively to estimating the systematic uncertainty inherent to the prediction Eqn. 7A by varying the parameters as discussed above, it is suggested in [36] to study the difference between the prediction Eqn. 5 based upon the colour-dipole model with predictions based upon parton-shower evolution, as e. g. Eqn. 3. Since this measurement of  $C_A/C_F$  is sensitive rather to the energy dependence of the multiplicities than to the absolute value of multiplicity, the uncertainty of Eqn. 5 is relevant here. Both predictions, Eqn. 3 and

$\kappa_{\text{Le}}$ [GeV]	$N_{gg} \pm(\text{stat.})\pm(\text{sys.})$	$\kappa_{\text{Le}}$ [GeV]	$N_{gg} \pm(\text{stat.})\pm(\text{sys.})$
13.36	$11.21 \pm 0.14 \pm 0.14$	35.26	$19.96 \pm 0.14 \pm 0.11$
15.57	$12.41 \pm 0.12 \pm 0.08$	38.01	$20.73 \pm 0.16 \pm 0.13$
17.82	$13.43 \pm 0.11 \pm 0.09$	40.69	$21.56 \pm 0.16 \pm 0.15$
20.13	$14.32 \pm 0.11 \pm 0.08$	43.37	$22.09 \pm 0.17 \pm 0.18$
22.50	$15.56 \pm 0.11 \pm 0.08$	45.87	$22.72 \pm 0.18 \pm 0.18$
24.92	$16.53 \pm 0.11 \pm 0.13$	48.19	$23.81 \pm 0.19 \pm 0.21$
27.45	$17.57 \pm 0.12 \pm 0.16$	50.19	$23.71 \pm 0.19 \pm 0.11$
30.01	$18.32 \pm 0.13 \pm 0.10$	51.69	$24.60 \pm 0.20 \pm 0.15$
32.61	$19.27 \pm 0.14 \pm 0.15$	52.50	$23.75 \pm 0.22 \pm 0.22$

Table 15:  $N_{gg}$  extracted from three-jet events with symmetric topologies

Eqn. 5 are shown in Fig. 13. The difference between the two predictions, evaluated at the centre of the data around  $\sim 40\text{GeV}$  is  $\sim 3.7\%$ . This corresponds to an one-sigma error-estimate of 2.1% which is completely compatible with the theoretical error given in Tab. 14. The result obtained with symmetric topologies is therefore

$$\frac{C_A}{C_F} = 2.257 \pm 0.019_{\text{stat.}} \pm 0.056_{\text{exp.}} \pm 0.070_{\text{theo.}} \quad (27)$$

and

$$\frac{C_A}{C_F} = 2.261 \pm 0.014_{\text{stat.}} \pm 0.036_{\text{exp.}} \pm 0.066_{\text{theo.}} \quad (28)$$

with general topologies. Both results are strongly correlated due to a large fraction of common events, so an average cannot be made here. Instead, the more precise result obtained with general topologies is taken as the central result. This result is the most precise measurement of the colour factor ratio so far with an overall relative uncertainty of 3.4%.

In Fig. 9 the colour factor ratios  $C_A/C_F$  and  $T_R/C_F$  are mapped for several symmetry groups where  $T_R = N_F T_F$  with  $N_F$  as the number of active quark flavours and  $T_F = 1/2$  as the normalisation of the SU(3) representation. In this plot the present analysis result is indicated by the shaded vertical band. The shaded diagonal band is the result of a measurement of the QCD  $\beta$ -function correlating  $T_R/C_F$  with  $C_A/C_F$  [37]. The dashed ellipses represent measurements of the four-jet cross section as function of the inter-jet angles [38]. The measurements are combined by adding their  $\chi^2$ -functions. The solid contour represents the  $\Delta\chi^2 = 2.4$  limit, corresponding to a confidence level of 68%. It is in excellent agreement with the QCD expectation of SU(3).

## 7 The extraction of $N_{gg}$

Instead of fitting  $C_A/C_F$  with the measured three-jet event multiplicities, the predictions of Eqn. 7A and Eqn. 7B can be used to extract the multiplicities of unrestricted two-gluon colour-singlet systems from the three-jet event multiplicity. As the direct experimental access to this quantity is severely limited, this proves to be an interesting option. The predictions Eqn. 7A and Eqn. 7B are solved for the gluonic contribution

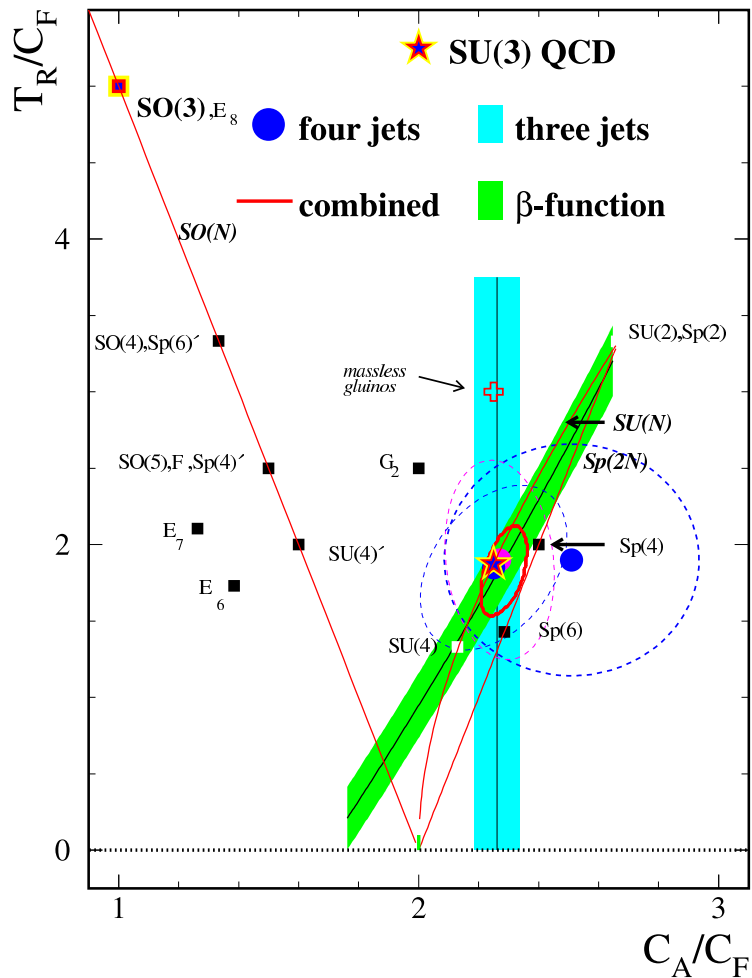


Figure 9: The plot shows the Casimir eigenvalues expected for the special orthogonal (SO(N), straight line on the left) and the special unitary (SU(N), curved line on the right) groups as well as for the symplectic groups (SP(2N), straight line on the right). E<sub>6</sub>, E<sub>7</sub>, E<sub>8</sub>, G<sub>2</sub> and F are the five exceptional Lie groups. The shaded bands and the dashed ellipses indicate the result of this and other [37,38] experimental analyses, which are combined in the solid ellipse.

yielding

$$N_{gg}(\kappa_{Le}) = 2 \cdot \left( N_{q\bar{q}g}(\vartheta_2, \vartheta_3) - N_{q\bar{q}}(L_{q\bar{q}}, \kappa_{Lu}) \right) \quad (29A)$$

$$N_{gg}(\kappa_{Lu}) = 2 \cdot \left( N_{q\bar{q}g}(\vartheta_2, \vartheta_3) - N_{q\bar{q}}(L, \kappa_{Lu}) \right) \quad (29B)$$

As discussed already in the previous section, Eqn. 7B fails to describe the data so only Eqn. 29A, which is based on Eqn. 7A, is used to extract the gluon multiplicity. The hadronisation correction discussed in Sect. 5 is taken into account by dividing  $N_{q\bar{q}g}$  by the appropriate correction factor.  $N_{q\bar{q}}$  is calculated for all three gluon-jet hypotheses and averaged with the appropriate weights as discussed above before subtracting it from the three-jet multiplicity. Analogously, the value of  $\kappa_{Le}$ , at which  $N_{gg}$  is being determined, is the weighted average of the  $\kappa_{Le}$ -values for the three possible gluon-jet hypotheses.

According to the procedure of Sect. 6 the angular ordered Durham algorithm is applied to obtain the central results. Also, only the topologies which entered the fit in Sect. 6

$\kappa_{Le}$ [GeV]	$N_{gg} \pm(\text{stat.})\pm(\text{sys.})$	$\kappa_{Le}$ [GeV]	$N_{gg} \pm(\text{stat.})\pm(\text{sys.})$
24.29	16.28 $\pm$ 0.09 $\pm$ 0.17	36.14	20.78 $\pm$ 0.12 $\pm$ 0.17
26.44	16.96 $\pm$ 0.09 $\pm$ 0.15	36.38	20.56 $\pm$ 0.12 $\pm$ 0.17
27.25	17.23 $\pm$ 0.28 $\pm$ 0.14	36.50	20.39 $\pm$ 0.14 $\pm$ 0.15
27.79	17.64 $\pm$ 0.10 $\pm$ 0.09	37.13	20.49 $\pm$ 0.11 $\pm$ 0.15
28.78	17.89 $\pm$ 0.10 $\pm$ 0.12	37.73	20.17 $\pm$ 0.38 $\pm$ 0.34
28.99	18.64 $\pm$ 0.33 $\pm$ 0.20	38.75	20.88 $\pm$ 0.11 $\pm$ 0.15
29.44	17.89 $\pm$ 0.10 $\pm$ 0.14	39.67	18.90 $\pm$ 1.19 $\pm$ 1.12
29.60	18.08 $\pm$ 0.10 $\pm$ 0.10	40.01	21.33 $\pm$ 0.12 $\pm$ 0.14
29.93	18.55 $\pm$ 0.10 $\pm$ 0.12	40.52	21.42 $\pm$ 0.12 $\pm$ 0.12
30.27	18.55 $\pm$ 0.11 $\pm$ 0.14	40.88	21.78 $\pm$ 0.13 $\pm$ 0.13
30.45	18.79 $\pm$ 0.11 $\pm$ 0.20	41.33	21.84 $\pm$ 0.18 $\pm$ 0.13
30.50	19.00 $\pm$ 0.17 $\pm$ 0.20	41.35	21.96 $\pm$ 0.13 $\pm$ 0.17
30.59	19.39 $\pm$ 0.11 $\pm$ 0.11	41.63	21.88 $\pm$ 0.13 $\pm$ 0.17
30.66	19.27 $\pm$ 0.13 $\pm$ 0.28	43.86	22.25 $\pm$ 0.09 $\pm$ 0.14
30.66	19.80 $\pm$ 0.16 $\pm$ 0.25	44.60	20.75 $\pm$ 0.59 $\pm$ 0.51
31.69	18.82 $\pm$ 0.10 $\pm$ 0.15	45.88	22.83 $\pm$ 0.09 $\pm$ 0.15
32.33	18.68 $\pm$ 0.32 $\pm$ 0.44	46.71	23.09 $\pm$ 0.13 $\pm$ 0.17
33.25	19.43 $\pm$ 0.10 $\pm$ 0.12	46.97	23.02 $\pm$ 0.10 $\pm$ 0.16
34.42	19.93 $\pm$ 0.11 $\pm$ 0.16	47.55	23.28 $\pm$ 0.10 $\pm$ 0.13
34.51	19.33 $\pm$ 0.55 $\pm$ 0.51	48.00	22.82 $\pm$ 0.46 $\pm$ 0.35
34.86	19.96 $\pm$ 0.11 $\pm$ 0.10	50.14	23.85 $\pm$ 0.15 $\pm$ 0.17
35.27	20.12 $\pm$ 0.11 $\pm$ 0.13	51.52	24.37 $\pm$ 0.18 $\pm$ 0.16
35.78	20.27 $\pm$ 0.12 $\pm$ 0.13	51.72	23.93 $\pm$ 0.12 $\pm$ 0.16
36.07	20.76 $\pm$ 0.20 $\pm$ 0.26		

Table 16:  $N_{gg}$  extracted from three-jet events with general topologies

are considered in order to provide a good description of the three-jet multiplicity by the prediction. As the additional multiplicity due to  $b$ -quark decays has been found to be topology independent,  $udscb$ -events are used in order to avoid the uncertainties inherent in the  $b$ -tagging procedure and  $N_0$  is fitted to the data yielding  $N_0 = 0.628 \pm 0.017$  for general and  $N_0 = 0.628 \pm 0.024$  for symmetric topologies with the  $\chi^2/N_{df}$  values of 80.4/74 and 7.3/17 respectively. The differences between the prediction and the measured three-jet event multiplicity are shown in Fig. 10. The agreement between data and prediction is good, especially for symmetric topologies. Anti- $b$ -tagged  $udsc$ -events, with  $N_0$  fixed at 0, are taken into account when estimating the systematic uncertainties of  $N_{gg}$ .

The gluon multiplicities obtained are given in Tab. 15 and Tab. 16. They are shown in Fig. 11 as a function of  $p_{t,Le}$  which has been identified with the centre-of-mass energy of the unrestricted two-gluon colour-singlet system. Solid circles indicate the results from symmetric, solid squares from general event topology. For clarity the multiplicities from general topologies have been rebinned in  $p_t$  in the upper plot. The unrebinning results are shown in the lower plot of Fig. 11. Results of both topology classes are found to be in good agreement. The good agreement between prediction and data in symmetric topologies also for small opening angles allows gluon multiplicities at small values of  $\kappa_{Le}$  to be obtained resulting in a larger kinematic range covered by the gluon multiplicities from symmetric than from general topologies.

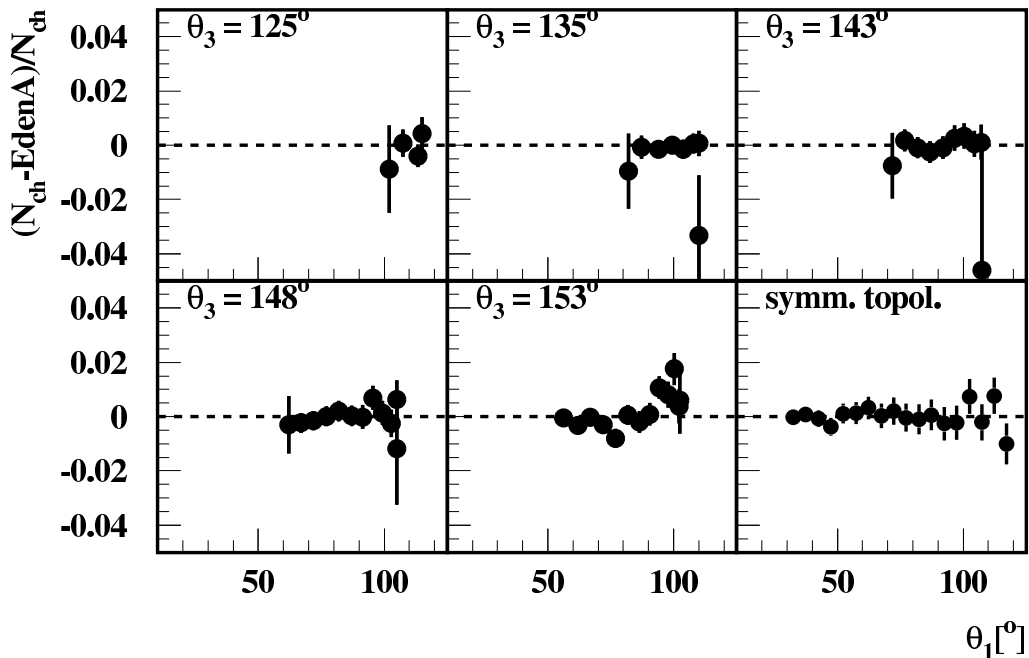


Figure 10: Difference between the measured three-jet event multiplicity and the prediction Eqn. 7A.

The solid line in Fig. 11 represents the prediction for the gluon multiplicity which has been described in Sect. 5. The agreement between this prediction and the extracted gluon multiplicities reflects the good description of the three-jet event multiplicities by Eqn. 7A. The measurement of  $N_{gg}$  of the CLEO collaboration at  $\sim 10$  GeV shown in Fig. 11 has been used to fix the constant of integration when setting up the prediction for  $N_{gg}$ , therefore it agrees by definition with the prediction. However, this value does not enter in the determination of  $N_{gg}$ . The measurement at  $\sim 5$  GeV is represented with statistical errors only. The OPAL measurement of  $N_{gg}$  around 80 GeV is based on the measurement of gluon jets recoiling against two identified  $b$ -quark jets [10]. The OPAL measurements at lower energies used identified gluon jets from three-jet events and an effective jet energy scale [12]. Also included is a measurement of the TOPAZ collaboration obtained from fully symmetric events [6]. The measurement [18] is not included in Fig. 11, as it is based on Eqn. 7B which has been found not to describe the data satisfactorily. The overall agreement between the several measurements is good.

After the preliminary presentation of the analysis of symmetric three-jet events in [17], a similar analysis has been published [18], where different conclusions have been reached. Especially the prediction Eqn. 7B has been preferred over Eqn. 7A due to the observed extrapolation behaviour of the extracted gluon multiplicities. However, only symmetric topologies have been studied in [18], while the main arguments of this analysis to disfavour Eqn. 7B compared to Eqn. 7A are the inconsistent results for symmetric and general topologies obtained when using Eqn. 7B. Moreover, the extrapolation behaviour of the gluon multiplicities extracted with Eqn. 7A to direct measurements at lower energies is satisfying, when a hadronisation correction is applied. Note that in [18] no hadronisation correction has been used and the extrapolation behaviour of the gluon multiplicities extracted using Eqn. 7A has been found to be unsatisfying, leading to the preference of

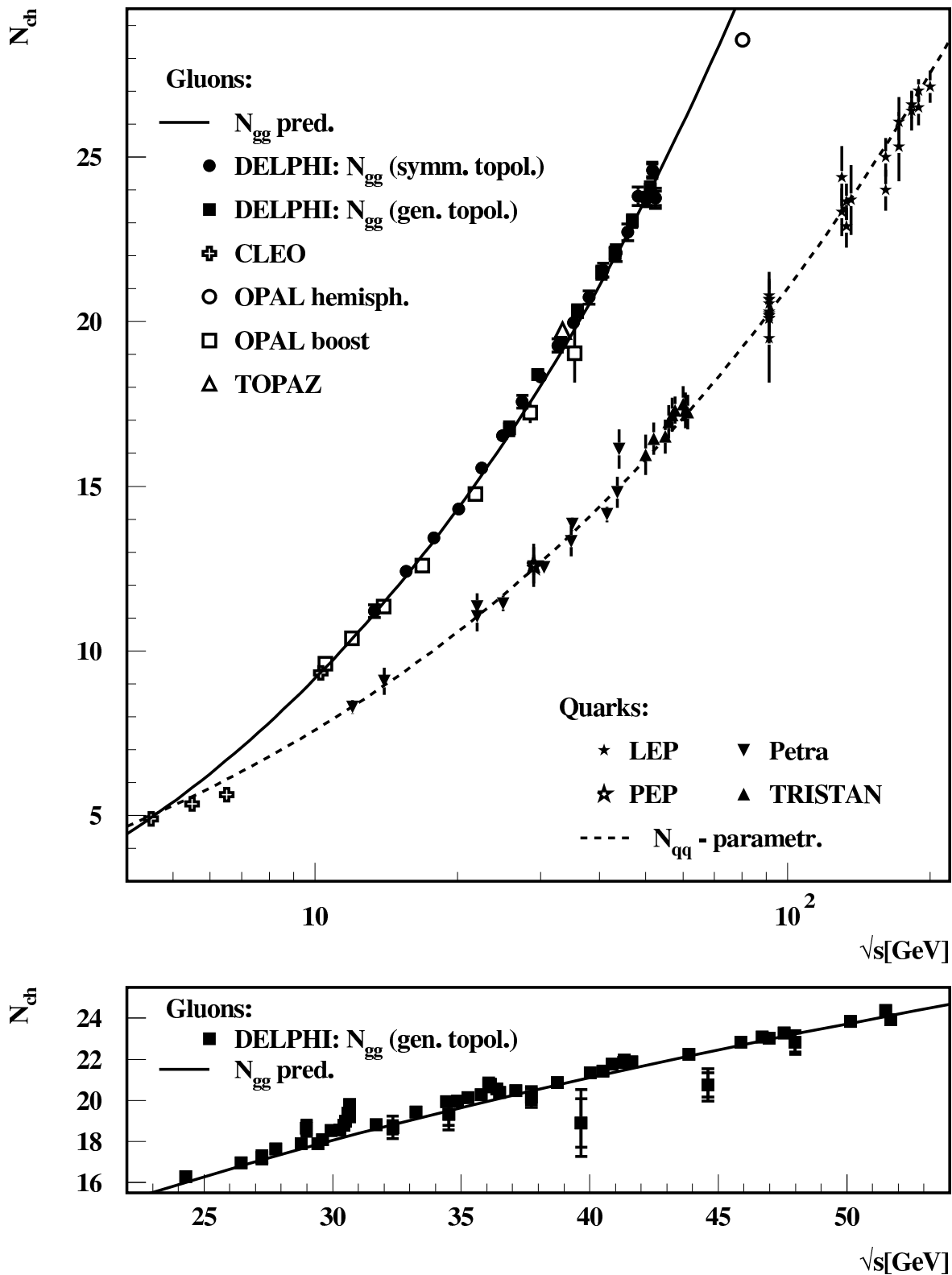


Figure 11: Gluon and quark multiplicities. For clarity, gluon multiplicities from general topologies are rebinned in the upper plot. In the bottom plot these Multiplicities are shown for each topology bin.

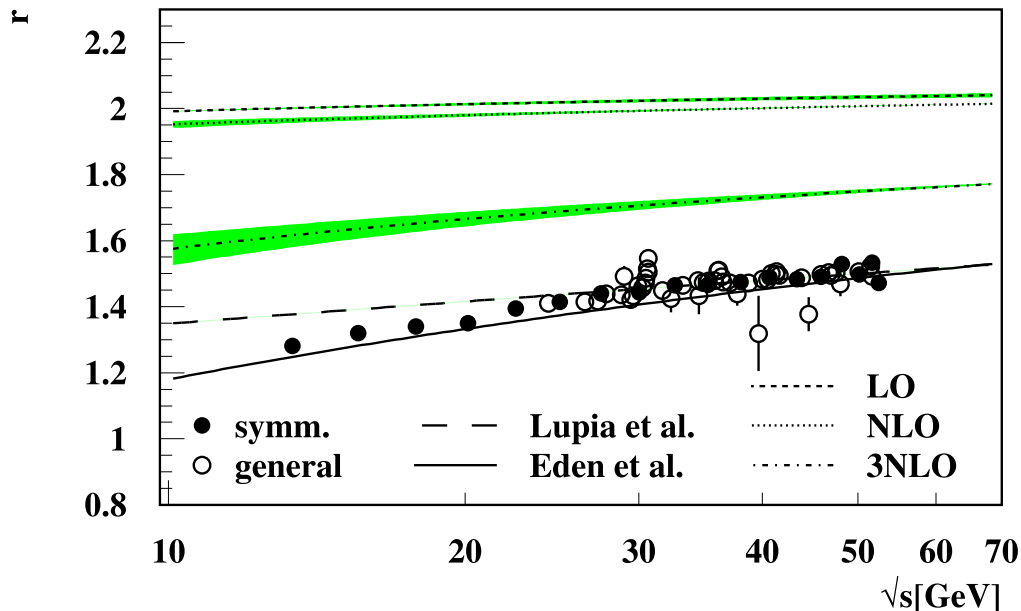


Figure 12: Measurements of  $r$  as defined in Eqn. 1 in comparison with theoretical predictions. The shaded bands indicate the effects of a variation of  $N_F$  between 3 and 5.

Eqn. 7B over Eqn. 7A in [18]. A more extensive attempt to compare both analyses can be found in [39].

In addition to the gluon multiplicity, in Fig. 11 the unrestricted  $q\bar{q}$ -multiplicity measured by several  $e^+e^-$  experiments which have been used to parametrise the prediction are shown. The measurements have been corrected for the varying  $b$ -contributions, so the multiplicity of  $udsc$ -events is shown. The line indicates the fitted parametrisation from Eqn. 9. The higher multiplicity and the larger slope of the gluon multiplicity with respect to energy in comparison with the  $q\bar{q}$  multiplicity can be clearly observed illustrating the observation of the larger colour charge of gluons.

In order to obtain the ratio  $r$  of the gluon and quark multiplicity, the extracted gluon multiplicities are divided by the parametrisation of  $N_{q\bar{q}}$  evaluated at the respective energy. The obtained values for  $r$  are shown in Fig. 12. Open dots represent the results from general, solid dots from symmetric topologies. The curves indicate the LO, NLO and 3NLO predictions of  $r$  discussed in Sect. 3 with the shaded area representing the effects of a variation of  $N_F$  between 3 and 5. Additionally, the result of a numeric calculation [40] is indicated. The predictions clearly overestimate the measured ratio. The overestimate is larger the lower the order of the calculation is. The difference between the predictions is also rather large. The reason for the poor description of the measurement by these predictions are non-perturbative effects to which the absolute value of multiplicity is especially sensitive. Only the line derived from the prediction of Eqn. 5 describes the data, but in the determination of this curve experimental input, especially the measurement of the gluon multiplicity at  $\sqrt{s} = 10$  GeV which fixes the constant of integration, enters, so this line includes a non-perturbative correction.

The ratio of the derivatives of gluon and quark multiplicity with respect to the energy,  $r^{(1)}$ , is expected to be less sensitive to such non-perturbative effects.  $r^{(1)}$  is obtained from the measured gluon multiplicities by taking the linear slope of mutually exclusive pairs of measured multiplicities which is then divided by the derivative of the parametrisation

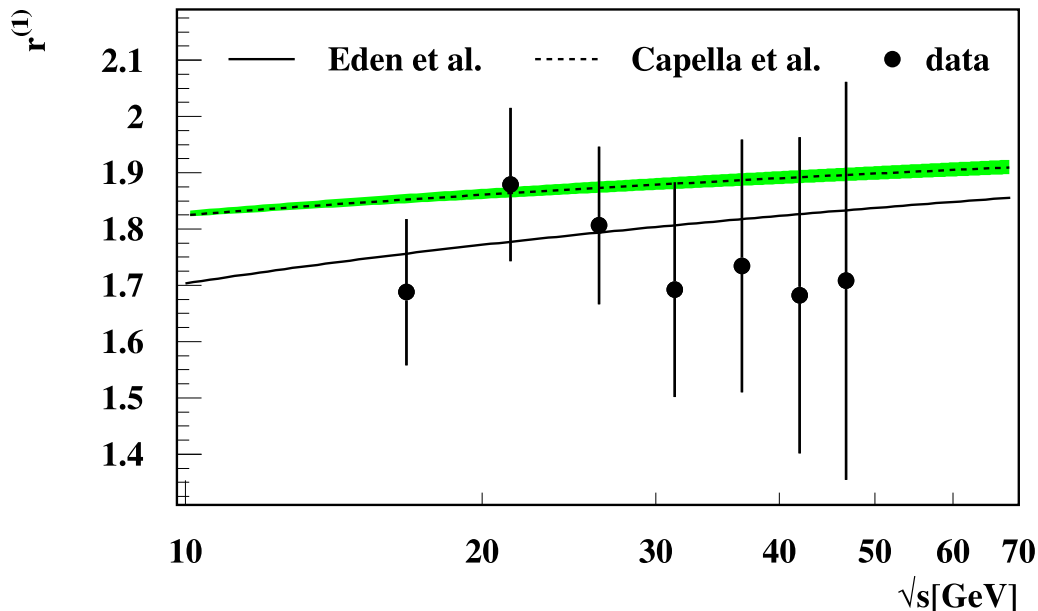


Figure 13: Measurements of  $r^{(1)}$  as defined in Eqn. 3 in comparison with theoretical predictions. The shaded bands indicate the effects of a variation of  $N_F$  between 3 and 5.

	$k$	$Q_0[\text{GeV}]$	$\chi^2/N_{df}$
$N_{q\bar{q}}$	$0.243 \pm 0.011$	$0.454 \pm 0.051$	0.75
$N_{gg}$	$0.1980 \pm 0.0005$		8.5
$N_{gg}$	$0.343 \pm 0.012$	$1.317 \pm 0.084$	1.1

Table 17: Parameter values of the 3NLO-fits of  $N_{q\bar{q}}$  and  $N_{gg}$

of  $N_{q\bar{q}}$  taken at the respective energy value. The obtained values for  $r^{(1)}$  are shown in Fig. 13. Only symmetric topologies have been considered here, as they cover a larger kinematic range and are more evenly distributed in energy. However, the results obtained from general topologies for  $r^{(1)}$  are in full agreement with the results shown in Fig. 13. The measured  $r^{(1)}$  are constant within their errors, the weighted mean is:

$$r^{(1)} = 1.75 \pm 0.07 \quad . \quad (30)$$

$r^{(1)}$  is therefore significantly higher than  $r$  due to the weaker dependence on non-perturbative effects, which reduce the ratio from the asymptotic value of  $C_A/C_F$ . The predictions Eqn. 3 and Eqn. 5 are indicated in Fig. 13 as curves. A reasonable agreement between the perturbative calculation and data can be observed here. Note that Eqn. 5 is a purely perturbative prediction for the slopes. Also the difference between both predictions is smaller for  $r^{(1)}$  than for  $r$ . Both observations confirm that the energy dependence of multiplicity is an observable superior to the absolute value of multiplicity.

The scale-independent values obtained for  $r^{(1)}$  already indicate that there is no direct sensitivity to the ratio  $r^{(2)}$  of the second derivatives of the multiplicities with respect to energy. However, the parametrisations of Eqn. 12 and Eqn. 13 can be fitted to the data and derivatives can then be obtained analytically. This procedure has already been applied in [18] in order to obtain  $r^{(2)}$ . As already observed in [3], the use of a common



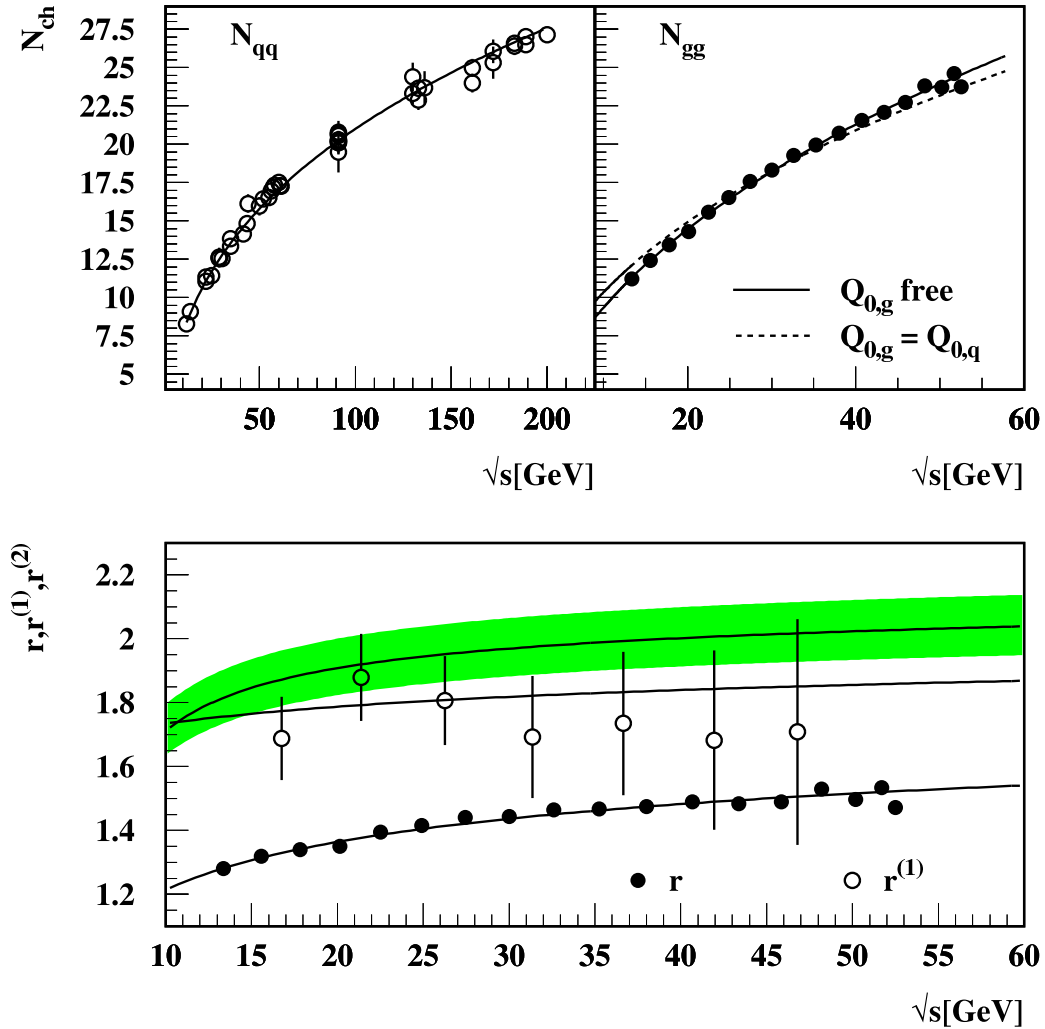


Figure 14: The top plots show the 3NLO predictions Eqn. 12 and Eqn. 13 fitted to the measured multiplicities. The lower plot shows from bottom to top  $r$ ,  $r^{(1)}$  and  $r^{(2)}$  which are derived from the fitted parametrisations together with the measured points for  $r$  and  $r^{(1)}$ .

normalisation  $k$  for quark and gluon multiplicity leads to a significant underestimation of the quark multiplicity and a wrong energy dependence. Therefore, the normalisations  $k_q$  and  $k_g$  are allowed to vary independently. As the quark multiplicities are measured more directly,  $Q_0$  is fixed by the fit of  $N_{q\bar{q}}$ . This leaves  $k_g$  as the only free parameter in  $N_{gg}$ . The values obtained for the parameters are given in Tab. 17, the fitted parametrisations are shown in the upper two plots of Fig. 14 as a solid line for  $N_{q\bar{q}}$  and as a dashed line for  $N_{gg}$ . The fit of  $N_{q\bar{q}}$  describes the data well, the value obtained for  $\chi^2$  is small and  $Q_0 = 454$  MeV is of the same order of magnitude as  $\Lambda_{\text{QCD}}$ . However, the energy dependence of the gluon multiplicity is not described well with this value of  $Q_0$ , the obtained  $\chi^2$  is quite large. Therefore,  $Q_0$  is also allowed to vary freely in the fit of  $N_{gg}$  resulting in two different effective energy scales for quarks and gluons. This apparently implausible finding can be motivated by the fact that due to the choice of evolution parameters leading to Eqn. 12 and Eqn. 13 both quantities are predicted not in exactly the same order leading to different effective scales. The variation of  $Q_0$  leads to a good description also of the gluon multiplicities by the prediction as indicated by the solid line in the upper right plot of Fig. 14, the parameter values obtained for  $N_{gg}$  are given in the last line of Tab. 17.

The derivatives of these fitted parametrisations can now be calculated analytically to any order and the ratios of these derivatives can be built. In the lower plot of Fig. 14 from bottom to top the ratios  $r$ ,  $r^{(1)}$  and  $r^{(2)}$  are shown in comparison with the measurements of  $r$  and  $r^{(1)}$ . The agreement between the measurement and the derived ratios is good, especially the energy dependence of  $r$  is well reproduced. The shaded area indicates the result obtained for  $r^{(2)}$  within the uncertainty given by the errors of the fit parameters. Interpreting this curve as a measurement of  $r^{(2)}$  the value obtained e.g. at 30 GeV would be found as

$$r^{(2)}(30 \text{ GeV}) = 1.97 \pm 0.09 \quad . \quad (31)$$

This value is in good agreement with the value obtained by a similar procedure in [18]. However, theoretical assumptions about the energy dependence of quark and gluon multiplicity are the basis of the parametrisations used, so that a theoretical bias cannot be avoided in obtaining this quantity.

## 8 Conclusions

The multiplicity of hadronic three-jet events has been measured as a function of variables depending on the event topology. A MLLA-prediction of this quantity has been fitted to the data yielding a measurement of the colour factor ratio

$$\frac{C_A}{C_F} = 2.261 \pm 0.014_{\text{stat.}} \pm 0.036_{\text{exp.}} \pm 0.066_{\text{theo.}} \quad .$$

With an overall relative uncertainty of 3.4% this is the most precise measurement of this quantity so far. It has been shown that the formulation Eqn. 7B of the prediction should be rejected in favour of the formulation Eqn. 7A. Using the MLLA-prediction to subtract the quark-contribution from the three-jet event multiplicity, the multiplicity of two-gluon colour-singlet systems has been extracted over a wide range of the effective energy scale. Comparing these multiplicities with the known multiplicities of quark-antiquark colour-singlet systems, the ratios  $r$ ,  $r^{(1)}$  and  $r^{(2)}$  have been studied. It has been found that  $r^{(1)}$  is an observable superior to  $r$  as non-perturbative effects affect the energy development of multiplicity less than the absolute value of multiplicity. However, the data do not show any significant sensitivity to the ratio  $r^{(2)}$ .

## Acknowledgements

We are greatly indebted to our technical collaborators, to the members of the CERN-SL Division for the excellent performance of the LEP collider, and to the funding agencies for their support in building and operating the DELPHI detector.

We acknowledge in particular the support of

Austrian Federal Ministry of Education, Science and Culture, GZ 616.364/2-III/2a/98, FNRS-FWO, Flanders Institute to encourage scientific and technological research in the industry (IWT), Belgium,

FINEP, CNPq, CAPES, FUJB and FAPERJ, Brazil,

Czech Ministry of Industry and Trade, GA CR 202/99/1362,

Commission of the European Communities (DG XII),

Direction des Sciences de la Matière, CEA, France,

Bundesministerium für Bildung, Wissenschaft, Forschung und Technologie, Germany,

General Secretariat for Research and Technology, Greece,

National Science Foundation (NWO) and Foundation for Research on Matter (FOM),

The Netherlands,

Norwegian Research Council,

State Committee for Scientific Research, Poland, SPUB-M/CERN/PO3/DZ296/2000,

SPUB-M/CERN/PO3/DZ297/2000, 2P03B 104 19 and 2P03B 69 23(2002-2004)

FCT - Fundação para a Ciência e Tecnologia, Portugal,

Vedecka grantova agentura MS SR, Slovakia, Nr. 95/5195/134,

Ministry of Science and Technology of the Republic of Slovenia,

CICYT, Spain, AEN99-0950 and AEN99-0761,

The Swedish Research Council,

Particle Physics and Astronomy Research Council, UK,

Department of Energy, USA, DE-FG02-01ER41155.

EEC RTN contract HPRN-CT-00292-2002.

## References

- [1] B.R.Webber, Phys. Lett. **B143** (1984) 501
- [2] J.B.Gaffney and A.H.Mueller, Nucl. Phys. **B250** (1985) 109
- [3] A. Capella et al., Phys. Rev **D61** (2000) 074009
- [4] MARK II collaboration, G. S. Abrams et al., Phys. Rev. Lett. **64** (1990) 1334,  
 ALEPH collaboration, D. Decamp et al., Phys. Lett. **B234** (1990) 209,  
 ALEPH collaboration, D. Decamp et al., Phys. Lett. **B273** (1991) 181,  
 ALEPH collaboration, D. Buskulic et al., Zeit. Phys. **C69** (1996) 15,  
 ALEPH collaboration, R. Barate et al., Phys. Rep. **294** (1998) 1,  
 DELPHI collaboration, P. Abreu et al., Zeit. Phys. **C50** (1991) 185,  
 DELPHI collaboration, P. Abreu et al., Zeit. Phys. **C52** (1991) 271,  
 DELPHI collaboration, P. Abreu et al., Eur. Phys.J. **C5** (1998) 585 ,  
 L3 collaboration, B. Adeva et al., Phys. Lett. **B259** (1991) 199 ,  
 L3 collaboration, B. Adeva et al., Zeit. Phys. **C55** (1992) 39,  
 OPAL collaboration, M. Z. Akrawy et al., Zeit. Phys. **C47** (1990) 505,  
 OPAL collaboration, P. D. Acton et al., Phys. Lett. **B291** (1992) 503,  
 OPAL collaboration, P. D. Acton et al., Zeit. Phys. **C53** (1992) 539 ,  
 OPAL collaboration, K. Ackerstaff et al., Eur. Phys.J. **C7** (1999) 369

- [5] TASSO collaboration, M. Althoff et al., Zeit. Phys. **C22** (1984) 307,  
TASSO collaboration, W. Braunschweig et al., Zeit. Phys. **C45** (1989)193 ,  
TPC/Two Gamma collaboration, H.Aihara et al., Phys. Lett. **B184** (1987) 299,  
MARK II collaboration, P. C. Rowson et al., Phys. Rev. Lett. **54** (1985) 2580,  
HRS collaboration, M. Derrick et al., Phys. Rev. **D34** (1986) 3304,  
AMY collaboration, H. W. Zheng et al., Phys. Rev. **D42** (1990)737,  
L3 collaboration, M. Acciarri et al., Phys. Lett. **B371** (1996) 137,  
DELPHI collaboration, P. Abreu et al., Phys. Lett. **B372** (1996) 172,  
OPAL collaboration, G. Alexander et al., Zeit. Phys. **C72** (1996) 191,  
ALEPH collaboration, D. Buskulic et al., Zeit. Phys. **C73** (1997) 409,  
OPAL collaboration, K. Ackerstaff et al., Zeit. Phys. **C75** (1997) 193,  
DELPHI collaboration, P. Abreu et al., Phys. Lett. **B416** (1998) 233,  
OPAL collaboration, G. Abbiendi et al., Eur. Phys. J. **C16** (2000) 185,  
DELPHI collaboration, P. Abreu et al., Eur. Phys. J. **C18** (2000) 203;  
Erratum ibid. **C25** (2002) 493
- [6] TOPAZ collaboration, K. Nakabayashi et al., Phys. Lett. **B413** (1997) 447
- [7] J. Fuster, K. Hamacher, O. Klapp, P. Langefeld, S. Marti and M. Siebel, contributed  
paper 545 to the International Europhysics Conference on High Energy Physics (EPS-  
HEP'97), Jerusalem 1997, DELPHI 97-81 CONF 67
- [8] DELPHI collaboration, P. Abreu et al., Z. Phys. **C70** (1996) 179
- [9] ALEPH collaboration, R. Barate et al., Z. Phys. **C76** (1997) 191
- [10] OPAL collaboration, G. Abbiendi et al., Eur. Phys. J. **C11** (1999) 217
- [11] DELPHI collaboration, P. Abreu et al., Eur. Phys. J. **C13** (2000) 573
- [12] OPAL collaboration, G. Abbiendi et al., Eur. Phys. J. **C37** (2004) 25
- [13] DELPHI collaboration, P. Abreu et al., Phys. Lett **B605** (2005) 37
- [14] DELPHI collaboration, P. Abreu et al., Phys. Lett. **B449** (1999) 383
- [15] P. Eden and G. Gustafson, JHEP **9809** (1998) 015, hep-ph/9805228
- [16] P. Eden, G. Gustafson and V. Khoze, Eur. Phys. J. **C11** (1999) 345, hep-ph/9904455
- [17] M. Siebel, K. Hamacher, P. Langefeld and O. Klapp contributed paper 640 to the  
International Conference on High Energy Physics, Osaka 2000  
CERN OPEN 2000-134
- [18] OPAL collaboration, G. Abbiendi et al., Eur. Phys. J. **C23** (2002) 597
- [19] DELPHI collaboration, P. A. Aarnio et al., Nucl. Instrum. Meth. **A303** (1991) 233
- [20] DELPHI collaboration, P. Abreu et al., Nucl. Instrum. Meth. **A378** (1996) 57
- [21] DELPHI collaboration, J. Abdallah et al., Eur. Phys. J. **C32** (2004) 185
- [22] Y. L. Dokshitzer et al., JHEP **9708** (1997) 001,  
S. Bentvelsen and I. Meyer, Eur. Phys. J. **C4** (1998) 623
- [23] S. Catani et al., Phys. Lett. **B269** (1991) 432
- [24] T. Sjöstrand, Computer Physics Comm. **82** (1994) 74
- [25] J. D. Bjorken and S .J. Brodsky, Phys.Rev. **D1** (1970) 1416
- [26] A. H. Mueller, Nucl. Phys. **B241** (1984) 141
- [27] I. M. Dremin and J. W. Gary, Phys. Lett. **B459** (1999) 341
- [28] Particle Data Group, S. Eidelman et al., Phys. Lett. **B592** (2004) 1
- [29] DELPHI collaboration, P. Abreu et al., Phys. Lett. **B347** (1995) 447
- [30] OPAL collaboration, R. Akers et al., Phys. Lett. **B352** (1995) 176
- [31] V.A. Khoze and W. Ochs, Int. J. Mod. Phys. **A12** (1997) 2949
- [32] K. Hamacher, Physics in Collision Zeuthen 2003 285-300  
**eConf C030626:SAAT08, 2003**

- [33] JADE collaboration, W. Bartel et al., Zeit. Phys. **C20** (1983) 187,  
PLUTO collaboration, C. Berger et al., Phys. Lett. **B95** (1980) 313,  
JADE collaboration, W. Bartel et al., Phys. Lett. **B88** (1979) 171
- [34] S. Kluth, Talk given at the XXXVIII. Rencontres de Moriond, 2003  
hep-ex/0305028
- [35] CLEO collaboration, M. S. Alam et al., Phys. Rev. **D46** (1992) 4822
- [36] P. Eden, Eur Ph J **C19** (2001) 493
- [37] DELPHI collaboration, J. Abdallah et al., Eur. Phys. J. **C29** (2003) 285
- [38] ALEPH collaboration, A. Heister et al., Eur. Phys. J. **C27** (2003) 1  
DELPHI collaboration, P. Abreu et al., Phys. Lett. **B414** (1997) 401  
OPAL collaboration, G. Abbiendi et al., Eur. Phys. J. **C20** (2001) 601
- [39] M. Siebel, PhD thesis, University of Wuppertal (WUB-DIS 2003-11),  
<http://elpub.bib.uni-wuppertal.de/edocs/dokumente/fbc/physik/diss2003/siebel>
- [40] S. Lupia and W. Ochs, Phys. Lett. **B418** (1998) 214